M2LW-24OR0402033

Light Water Reactor Sustainability Program

Progress on Dissolved Oxygen Effects Evaluation on the Stress Corrosion Cracking Initiation Susceptibility of Stainless Steel in PWR Primary Water

Ziqing Zhai
Mychailo Toloczko
Pacific Northwest National Laboratory

September 2024
U.S. Department of Energy
Office of Nuclear Energy

M2LW-24OR0402033

Progress on Dissolved Oxygen Effects Evaluation on the Stress Corrosion Cracking Initiation Susceptibility of Stainless Steel in PWR Primary Water

Ziqing Zhai
Toloczko Mychailo
Pacific Northwest National Laboratory

September 2024

Light Water Reactor Sustainability Program
Materials Research Pathway

http://lwrs.inl.gov

Prepared for the
U.S. Department of Energy
Office of Nuclear Energy
Under DOE Idaho Operations Office
Contract DE-AC07-05ID14517

Page intentionally left blank

ABSTRACT

About 90% of the primary components in pressurized water reactors are made of stainless steels. Operational experience with these stainless steels has generally been very good given their extensive use. Nevertheless, stress corrosion cracking (SCC) cases of unirradiated austenitic stainless steels in pressurized water reactor (PWR) primary water have occurred in the field since the early 1980s [1] and continued to this day. In particular, the more than 170 intergranular (IG) SCC cases reported since 2021 in stainless steel auxiliary piping of multiple French nuclear power plant (NPP) units suggest that austenitic stainless steels are not immune to IGSCC in free-flowing, non-contaminated primary water, and can occur in non-isolable portions of branch piping in the PWR primary circuit, posing threat to nuclear safety and leading to significant financial loss. While weld residual stress has been considered to play a key role in these incidents, it is also recognized that high residual stress alone is insufficient in causing the magnitude of IGSCC cases detected to date. The SCC initiation mechanisms remain largely convoluted due to the complex welding history, operating conditions, and metallurgical characteristics, requiring more systematic studies to determine the effect of each key influencing factor and their interactions. The current study is established to address this need, and this report summarizes the first-year research activities performed for this study, including materials preparation, characterization, and SCC initiation testing to evaluate the effect of dissolved oxygen on the SCC initiation susceptibility of cold forged 304L in 300°C PWR primary water. Two constant load SCC initiation tests have begun on 10–40% cold forged 304L blunt notch compact tension (BNCT) specimens in 300°C PWR primary water containing either 2 ppm dissolved oxygen (DO) or 50 ppb DO. The crack extension response of all specimens is being monitored in-situ by direct current potential drop (DCPD) for crack initiation detection. To date, both tests have accumulated 800+ hours of exposure at an estimated stress intensity of 30 MPa√m with no DCPD indication of SCC initiation in any of the specimens.

Page intentionally left blank

ACKNOWLEDGMENTS

The authors gratefully acknowledge the financial support from the U.S. Department of Energy, Office of Nuclear Energy, through the Light Water Reactor Sustainability Program Materials Research Pathway. In addition, Dr. Raul Rebak and Mr. Steve Buresh from G.E. Global Research Center are acknowledged for cold forging the 304L and 316L used in this study. Dr. Jared Smith at Electric Power Research Institute is acknowledged for technical discussions. Dr. Benjamin Schuessler is acknowledged for performing electron backscatter diffraction analysis on cold forged 304L materials. Key technical assistance from Robert Fluor, Dexter Kling, Michael Blazon, Nate Brown, and Irving Brown at Pacific Northwest National Laboratory is acknowledged for testing and materials preparation activities.

Page intentionally left blank

CONTENTS

FIGURES

TABLES

Page intentionally left blank

ACRONYMS

ASN	Autorité de Sûreté Nucléaire
BNCT	Blunt notch compact tension
BSE	Backscattered electron
CW	Cold worked
DCPD	Direct current potential drop
DC	Dislocation channels
EBSD	Electron backscatter diffraction
EdF	Electricité de France
FY	Fiscal year
GEGRC	General Electric Global Research Center
GB	Grain boundary
HAZ	Heat affected zone
IG	Intergranular
K	Stress intensity
NPP	Nuclear power plant
PWR	Pressurized water reactor
PWROG	Pressurized Water Reactor Owners Group
RHR	Residual heat removal
SCC	Stress corrosion cracking
SE	Secondary electron
SEM	Scanning electron microscope
SI	Safety injection
SS	Stainless steel
YS	Yield strength

Page intentionally left blank

Progress on Dissolved Oxygen Effects Evaluation on the Stress Corrosion Cracking Initiation Susceptibility of Stainless Steel in PWR Primary Water

1. Project Background

1.1 Objective

The first objective of the light water reactor sustainability (LWRS) task at Pacific Northwest National Laboratory (PNNL) is to identify underlying mechanisms controlling stress corrosion cracking (SCC) initiation and other possible long-term degradation modes that can potentially degrade SCC resistance in Ni-base alloys. Understanding and modeling the fundamental processes causing crack nucleation is a key step in predicting and mitigating SCC in the primary and secondary water systems of light water reactors (LWRs). It is also important to understand the long-term microstructural stability and performance of these alloys as a crucial step moving forward to fulfill their promise for broader applications in LWRs. Mechanistic information obtained could provide key insights to mitigate or control SCC in these materials, optimize inspection and maintenance schedules for the most susceptible materials and locations, and potentially define SCC-resistant materials. The second objective of this task is to evaluate the impact of emerging technologies proposed for sustaining reliable and economical operation of LWRs on SCC resistance of Ni-base alloys. The research scope is defined with regulatory and industry needs and is linked to state-of-the-art laboratory testing and microscopic characterizations.

1.2 Focus of Current Report

Type 304 and 316 austenitic stainless steels are the most widely used grades of stainless steels in pressurized water reactors (PWRs), mainly for structural supports of the reactor core and pressure-retaining boundary components such as piping in the primary circuit. Operational experience with these stainless steels has generally been very good given their extensive use, with the major concern being raised on the irradiation effects on core support structures. Nevertheless, stress corrosion cracking (SCC) cases of unirradiated austenitic stainless steels in PWR primary water have occurred in the field since the early 1980s [1] and continued to this day. Before the year 2020, a total of ~180 SCC events were reported worldwide on austenitic stainless steels exposed to primary water environments in PWRs. The majority of the events (~84%) occurred in low-flow regions or occluded/stagnant primary water conditions. However, in August 2020, an intergranular (IG) SCC crack was reported in the pressurizer spray line piping 316 stainless steel weldment in Japanese Ohi Nuclear Power Plant (NPP) Unit 3. Since October 2021, IGSCC cracks have been detected in stainless steel (SS) auxiliary piping systems in multiple French NPPs, causing at least twelve French nuclear power reactor units to go offline in 2021-2022 for inspection. In two years, the newly detected SCC cases reached a similar number of the total cases reported over the last 30 years worldwide. These new IGSCC cases detected in Japanese and French NPPs all occurred in free-flowing, non-contaminated PWR primary water and represent the first SCC cases confirmed in non-isolable portions of branch piping [2] in the PWR primary circuit, suggesting that IGSCC of austenitic stainless steels in PWR environments is a potentially serious emerging issue. Although no IGSCC incidents have been reported in analogous welds in U.S. PWRs, it is essential to have a better mechanistic understanding of the condition under which such IGSCC incidents could take place, so that informed inspection and maintenance plan can be made to prevent such events from jeopardizing plant operation.

To devise an adequate test plan to address such a need, a literature review was performed on relevant operational experience and associated laboratory research on the SCC of unirradiated austenitic SCC in PWR primary water in fiscal year (FY) 2023 and the information was summarized in [3]. The current report documents the actual testing effort started in FY 2024 focusing on the effect of dissolved oxygen (DO) on SCC initiation of stainless steels in PWR primary water. Chapter 1 gives a brief review of the IGSCC cases reported in the French NPPs with updates obtained in FY 2024 to provide a better understanding of the motivation of this study and the context of testing parameter selection. Chapter 2 introduces the materials purchased for this study and summarizes the mechanical property and microstructural characteristics of 304L, the focused testing material in FY 2024. Chapter 3 summarizes the test progress to date on the evaluation of the effect of dissolved oxygen content on the SCC initiation of cold worked 304L.

2. Background of the Study

2.1 Motivation

In October 2021, flaw indications were detected in the safety injection (SI) lines connected to the cold leg of the primary circuit at Civaux-1 during the second decennial outage [4]. The SI system is used to control accidents in which coolant escapes from the primary system due to a leak [5]. In French PWRs, it consists of a low-pressure and a medium-pressure injection systems as well as the pressure accumulators (Figure 1). It is connected in several places to the loops of the primary system, through which the water heated in the reactor core is fed into the steam generator and then cooled and returned to the reactor core [5]. The flaws were detected near two circumferential welds in an elbow weld joint made of non-sensitized 316LN, exposed to free-flowing, non-polluted hydrogenated primary water at ~300°C (Figure 2). The inspection method used was the standard mono-element ultrasonic technique dedicated to the identification of thermal fatigue cracks. To confirm the flaw indications, Electricité de France (EdF) cut out the impacted elbow weld joints and performed destructive examinations on them. The results unexpectedly revealed that the cracks detected in both weld joints are SCC instead of thermal fatigue cracks given their fully intergranular morphology (Figures 03 and 04). It should be noted that these cracks occurred in the portion of the piping immediately adjacent to the primary circuit piping, downstream of the SI isolation valves [6]. This implies that the leak cannot be isolated if it occurs at this location.

These cracks exhibit a circumferential orientation with a large aspect ratio (surface length >> depth) in the weld heat affected zone (HAZ). As shown in Figures 03 and 04, these elbow welds both have a very large root pass, but the subsequent passes were annealed during welding, which is believed to introduce compressive residual stress in the adjacent base metal [2]. This welding procedure may help explain the wider profile of elevated hardness values measured from the inner face (Figure 3) [7]. The fact that the crack did not grow deeper beyond the root pass also seems consistent with the quick drop in hardness measured from the inner surface near the subsequent passes. It is worth noting that the highest hardness values measured in these two welds did not exceed 270 HV, which is below the 300 HV previously identified as the threshold value based on operational experience for SCC initiation to occur in PWR primary water [8].

Upon detection of the above IGSCC incident in Civaux-1, EdF subsequently shutdown multiple NPPs for investigations of defect alike, and additional indications were detected in multiple units at the time of this report: Civaux-2, Chooz-1 & -2, Penly-1, Chinon-3, Cattenon-3, Flamanviller-2, and Golfech-1. These crack indications mostly occurred in SI lines and residual heat removal (RHR) lines in N4 (1450 MW) and P4 (1300 MW) type reactors, but not in the older, 900 MW plants [9]. The largest SCC crack detected thus far was found in Penly-1 in the HAZ of a weld in a SI line connected to the hot leg of the primary circuit. As shown in Figure 5, this weld was fully emerged in ~300°C deaerated primary water insusceptible to thermal stratification effects but was repaired twice during manufacturing [4]. By the time it was detected, the crack had grown to a circumferential length of 155 mm (~1/4 circumference) and a maximum depth of 23 mm (85% through-wall thickness) [4]. Figure 6 shows another IGSCC crack observed in an elbow weld joint in a cold leg of the SI system. The weld build-up showed a very different morphology than those reported in Civaux (Figures 03 and 04), highlighting the variability in welding practices among the welds in auxiliary piping systems.

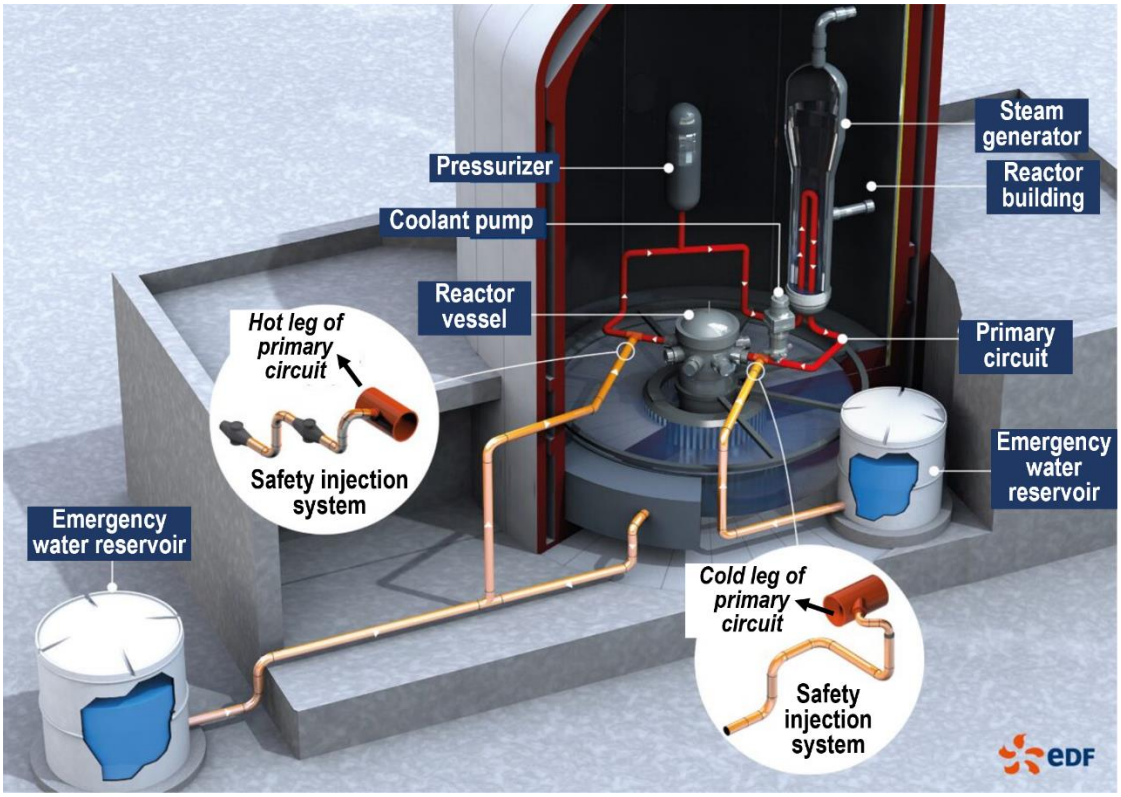

Figure 1. Illustration of the safety injection system location in the French N4 PWR design, redacted for English based on [10].

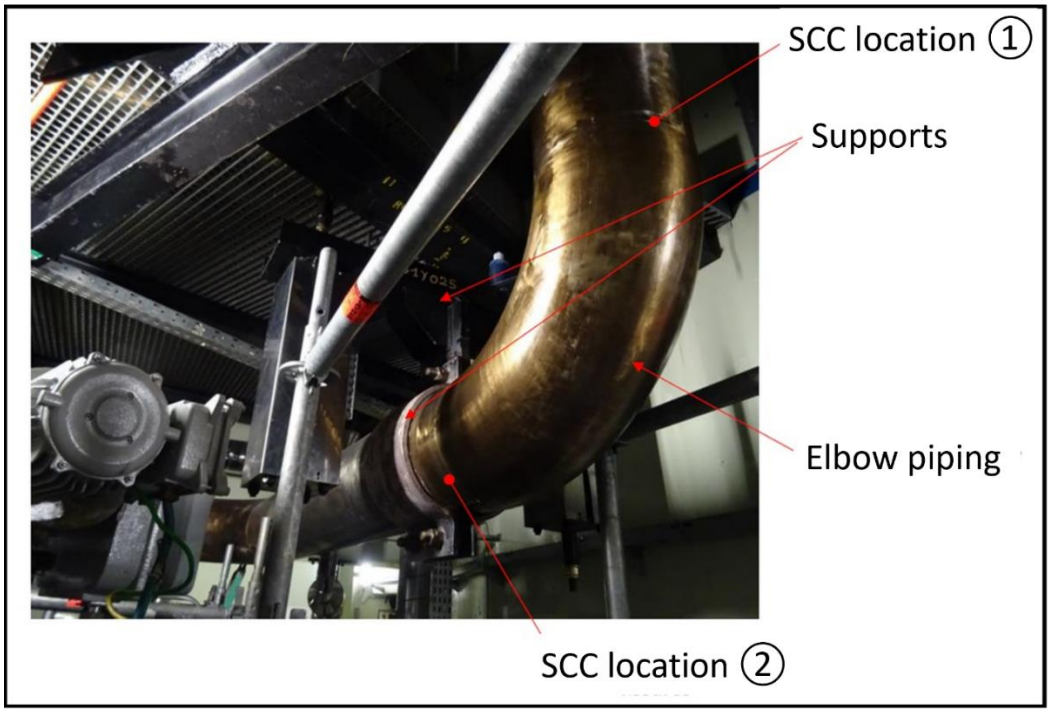

Figure 2. Photo of the actual elbow piping in a cold leg of the safety injection lines in Civaux-1 where the first SCC incidents were reported [11].

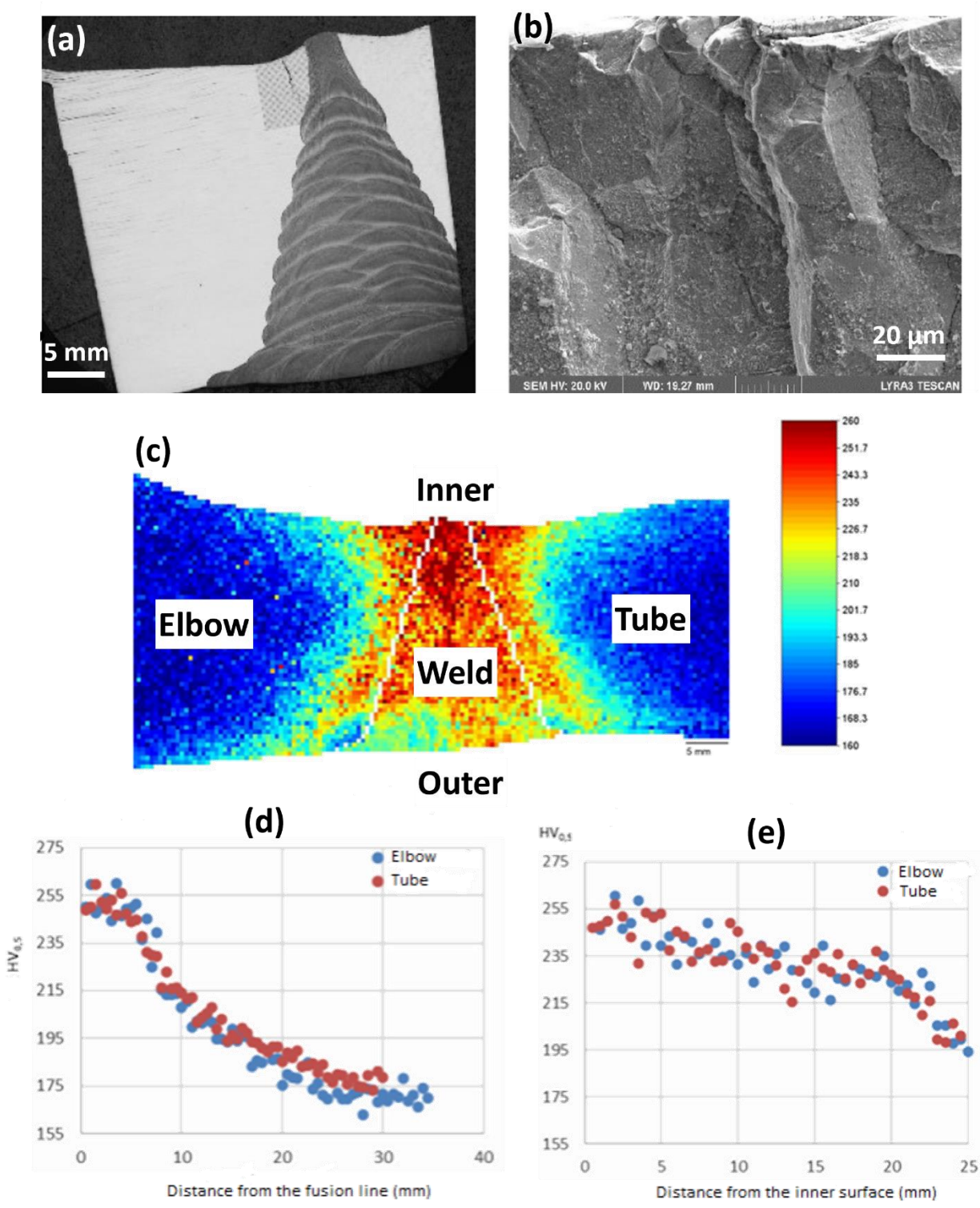

Figure 3. (a, b) Destructive examination and (c–e) hardness measurements of a cross-section containing the SCC crack found in location ① in Figure 2 [7].

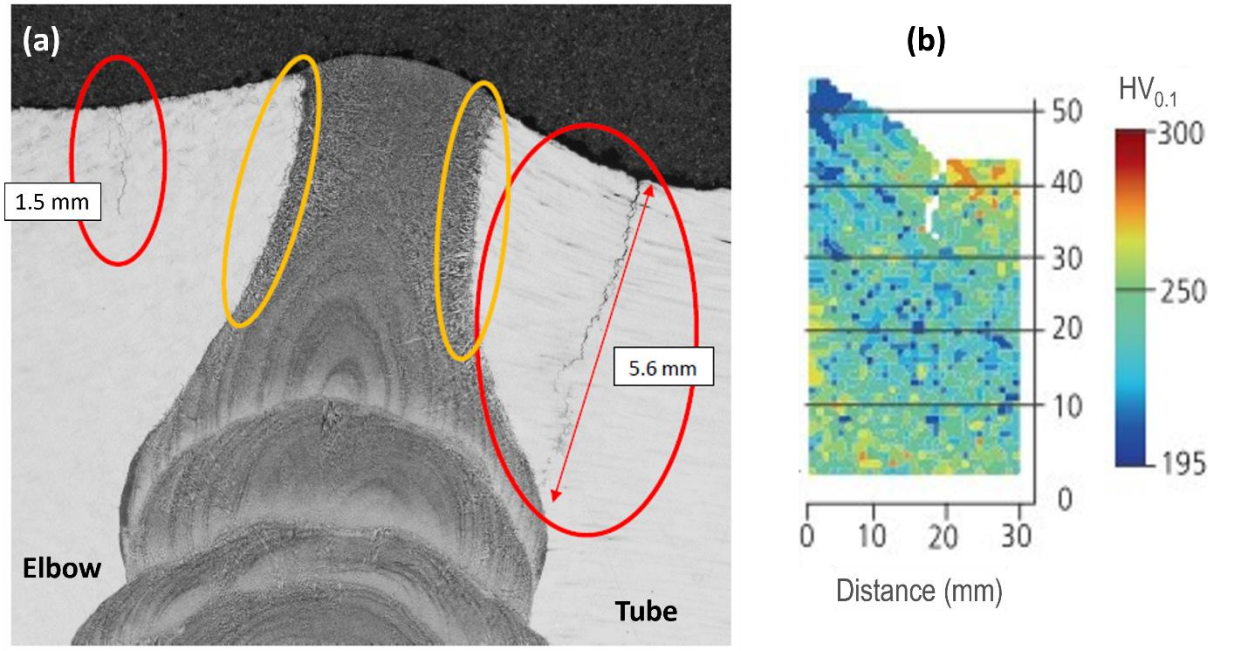

Figure 4. (a) Destructive examination of a cross-section containing the SCC cracks found in location ② in Figure 2, and (b) hardness map including part of the weld, HAZ, and base metal of the tube side. The location where the 5.6 mm-long crack is marked in (a) appears to coincide with the high-hardness area measured near the inner surface [12].

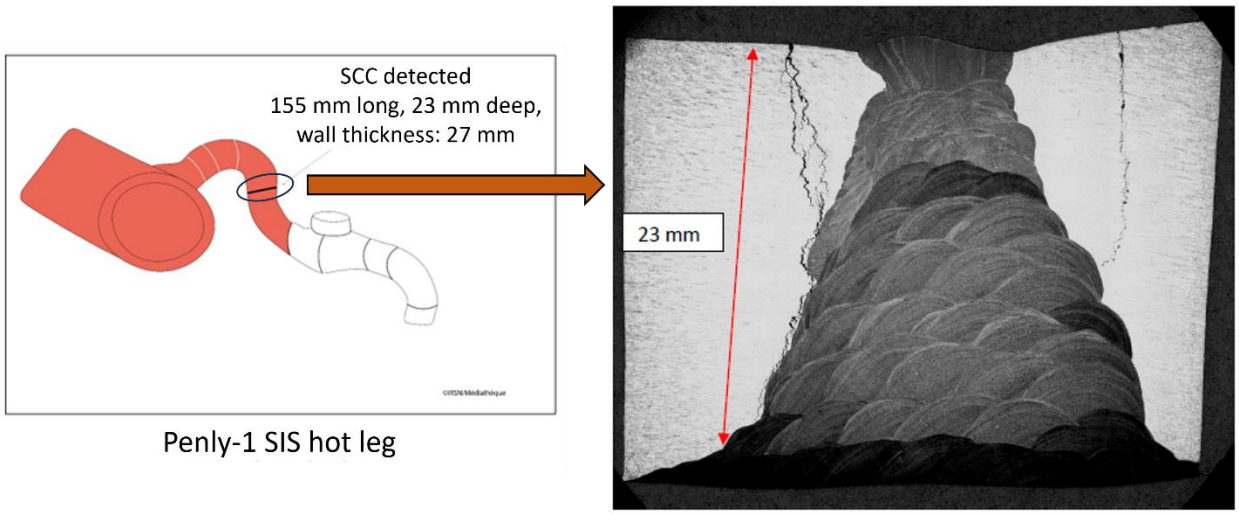

Figure 5. The longest SCC reported to date in all French PWRs. It was located in the HAZ of a weld joint in a hot leg of the safety injection system in Penly-1 (left) [4]. A micrograph of its morphology in the cross-section is also provided [13].

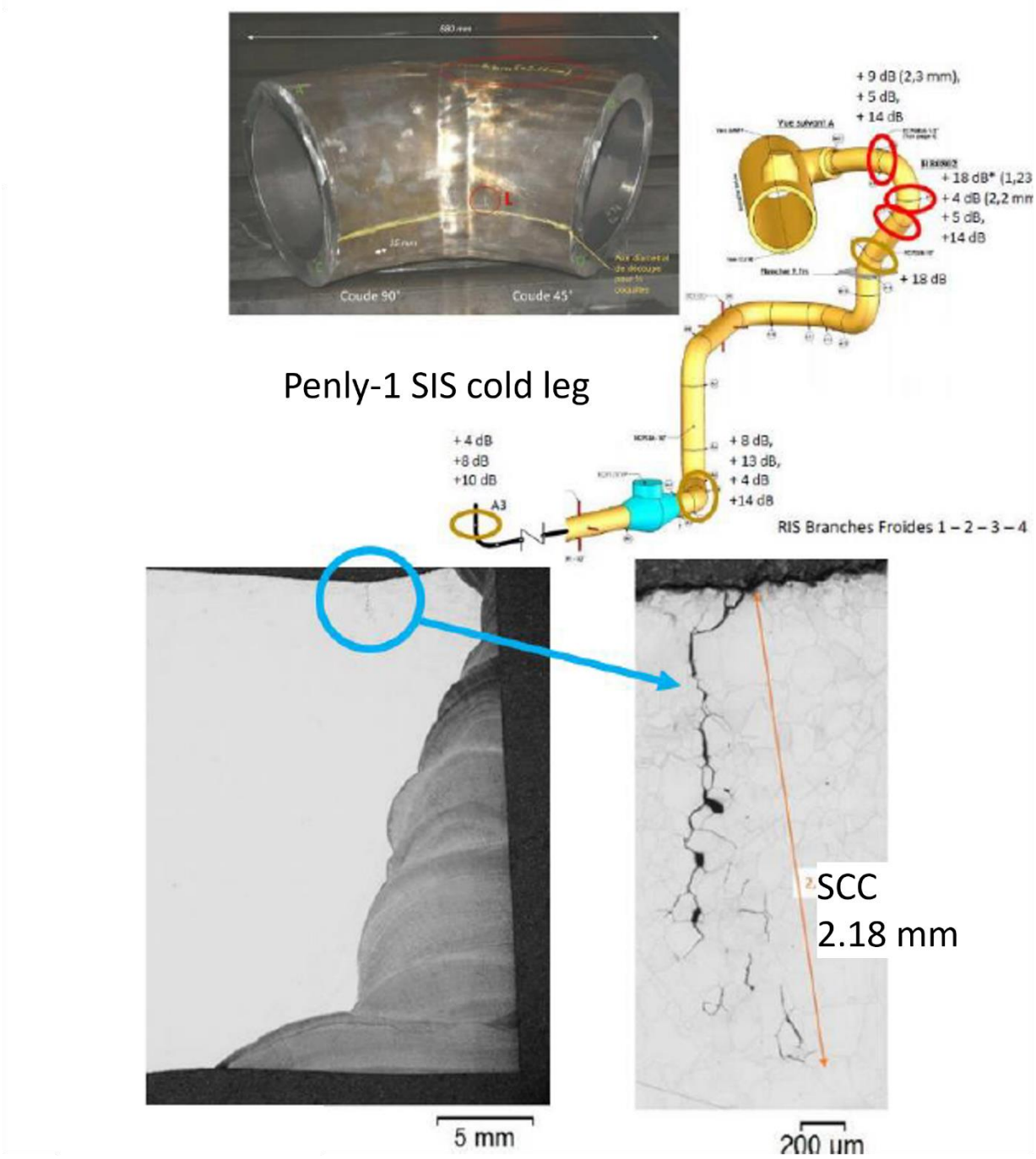

Figure 6. Example of destructive examination confirming the existence of SCC after defect indications were detected by ultrasonic technique in an elbow weld of a cold leg of the SI line in Penly-1 [14].

To date, additional inspections and investigations are still ongoing at EdF. Between the end of 2021 and June 2023, around 500 welds were inspected on the stainless steel welds of emergency core cooling systems and RHR systems across many French PWR units. The inspection used a new ultrasonic technique developed specifically for IGSCC detection and sizing, and ~200 welds were removed for laboratory examination. Figure 7 provides a summary of the frequency distribution of the examined IGSCCs as a function of their measured depth. A total of 172 IGSCC cases were summarized in this plot. It is worth noting that before the year 2020, a total of ~180 SCC events were reported worldwide on

austenitic stainless steels exposed to primary water environments in PWRs. The majority of the events (~84%) occurred in low-flow regions or occluded/stagnant primary water conditions. In two years, the newly detected SCC cases in French PWRs alone has reached a similar number of the total cases reported over the last 30 years worldwide, and all in free-flowing, non-contaminated PWR primary water.

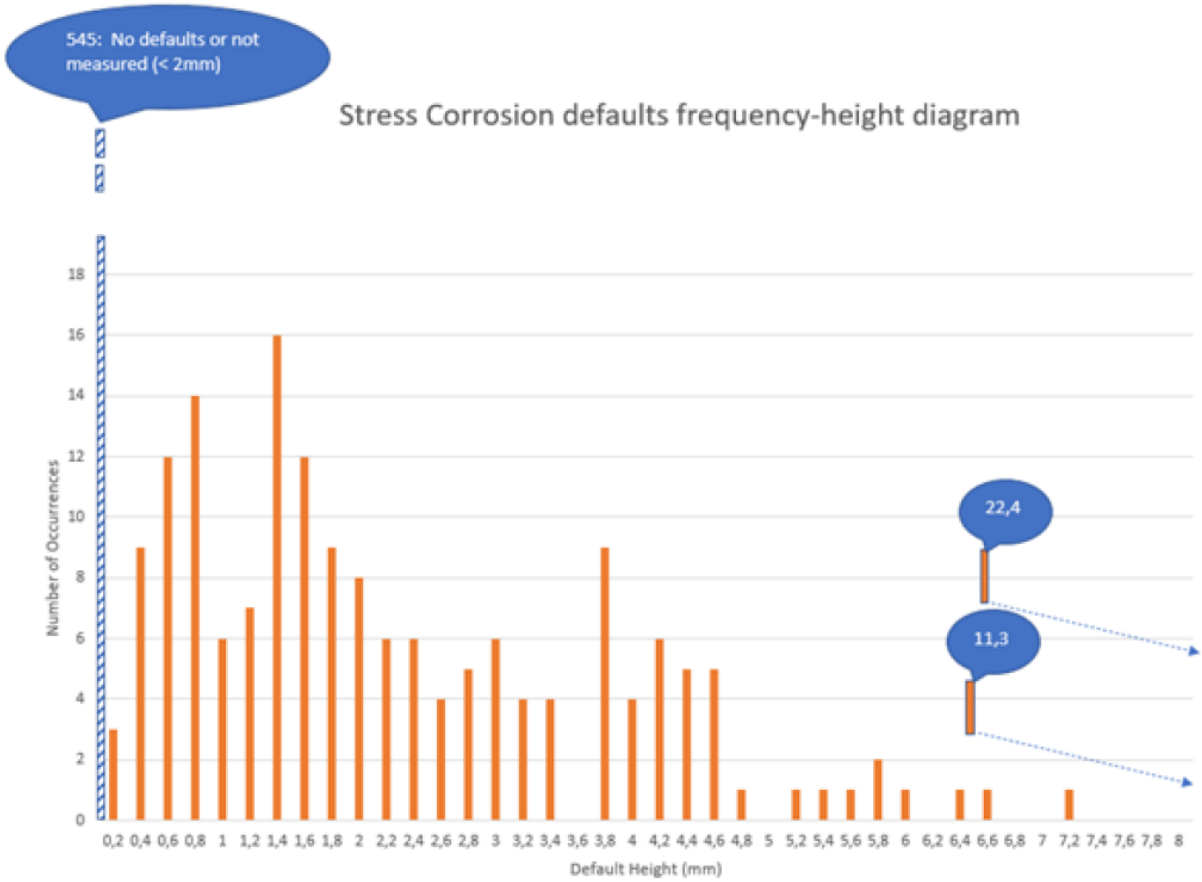

Figure 7. Distribution of IGSCC cracks depth (in mm) on emergency core cooling systems and RHR system welds examined between the end of 2021 and the beginning of 2023 in French PWRs [13].

As shown in Figure 7, most of these detected IGSCC remained shallow, with only two cracks exceeding a depth of 10 mm, and another nine cases exhibiting IGSCC cracks between 5 to 10 mm deep. Both welds made of 304L and 316L exhibited cracks. According to the manufacturing reports, various types of welding methods were used on the welds with IGSCC cracks including automated or tungsten inert gas welding, shielded metal arc welding, or flux welding. On some welds, a combination of these methods was used [13]. No specific welding method was found to be the most susceptible to SCC, but there are indications that automated process tends to create deeper cracks [15]. The fact that the cracks did not grow deeper is likely associated with decreasing weld residual stress from inner surface to the outer surface. However, questions remain on the cause of the initiation of these SCC cracks. According to the Autorité de Sûreté Nucléaire (ASN), elevated stresses caused by cyclic loading due to thermal stratification are suspected to be the primary contributor [2], followed by weld residual stress and potentially elevated oxygen due to dissolved oxygen in make-up water [16].

Statistics have shown that the pipes with the highest number of IGSCC cracks have a specific geometry that allows the thermal stratification phenomenon to occur, as illustrated in Figure 8. The water circulation within the main primary pipes generates a vortex that penetrates into the auxiliary pipe. The

water in the auxiliary pipe is, therefore, at the same temperature as the main primary pipes in the length that is penetrated by the vortex. If the vortex ends up in a horizontal part of the pipe, there is a superposition of a cold and a hot water layer inducing a bending stress. This additional stress in operation resulting from thermal stratification can likely explain the higher susceptibility of some particular pipe designs to IGSCC or fatigue cracks [13]. Another indirect evidence of the key role of thermal stratification is that the SCC occurrence has a strong dependence on reactor types. As shown in Table 1, the CP-type reactors and P4-type reactors have shown limited or no susceptibility to IGSCC due to the different geometry of the SI and RHR lines. The thermal stratification phenomenon is also relevant to the U.S. PWR fleet. The Pressurized Water Reactor Owners Group (PWROG) has reviewed the fleet branch piping configurations and identified those that meet the EDF criteria for susceptibility to thermal stratification. While such configurations are rare in SI piping, they are common for RHR suction piping. Thermal fatigue cracks are a known issue in such configurations and corresponding inspection procedure is in place, with no IGSCC cases reported to date.

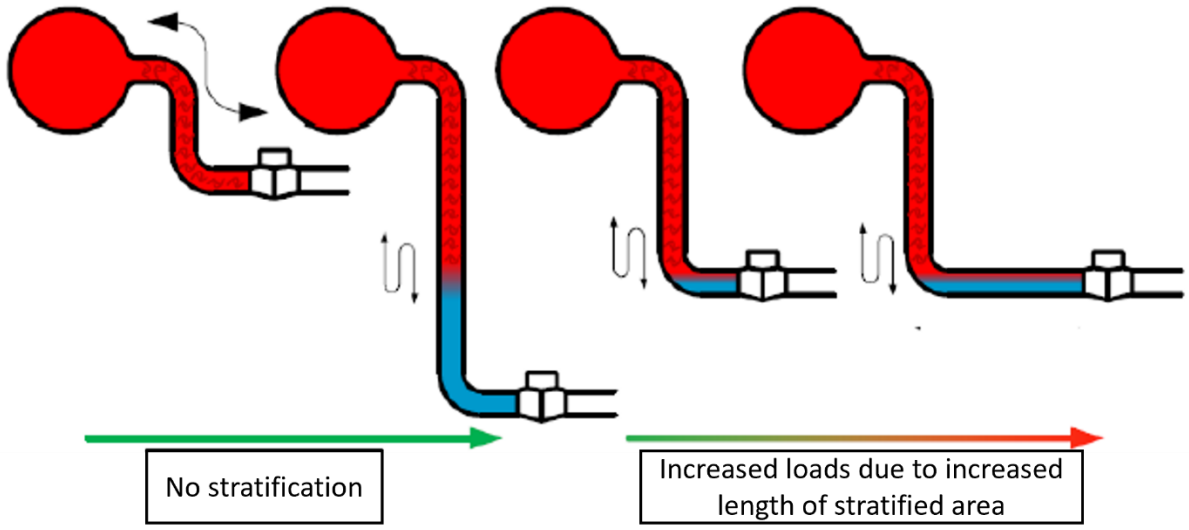

Figure 8. Illustration from EdF showing the effect of an auxiliary pipe design on thermal stratification [13].

Table 1. The systems and portions of their piping that were found sensitive to SCC on the PWR reactors of the French fleet [6].

Reactor System	**N4-type 1450 MW (4 reactors)**	**P'4-type 1300 MW (12 reactors)**	**P4-type 1300 MW (8 reactors)**	**CP0 and CP1-type 900 MW (32 reactors)**
Safety injection system	Lines connected to the cold leg of the primary loop	Lines connected to the cold leg of the primary loop	/	/
Residual heat removal system	Lines connected to the hot leg of the primary loop	/	/	/

However, there are cases where deep IGSCC was developed in absence of thermal stratification effect, such as the one reported in Penly-1 (Figure 5). In addition, it is interesting to note that many more IGSCC cases were found in lines connected to the cold leg than to the hot leg of the primary loop (Table 1), where the temperature is lower. Combined with the fact that the HAZ regions where the IGSCC occurred usually exhibit moderate hardness values lower than 300 HV (Figures 03 and 04), it is possible that other factors may have played a non-trivial role in causing SCC initiation to happen in these welds. The ASN suspects that DO in the primary water may have contributed to the observed SCC cases because there is a growing practice at EdF not to deaerate the make-up water tanks connected to the primary circuits, making it possible to have aerated water entering safety injection systems, resulting in discontinuous oxygen ingress. The scenarios, however, are very complicated and only postulated. Depending on the geometry of the piping, there are cases where aerated make-up water is injected only meters upstream, leaving only a fraction of a second for mixing before reaching the regions where SCC was reported thus extremely short oxygen transients. There is also the possibility of non-homogeneous mixing when a slug of cold water is injected into a hotter flowing stream leading to thermal stratification with examples shown in Figure 8, providing longer transients for oxygen ingress. Besides these scenarios, occluded crevice, if present, can also trap oxygen and lead to high local DO concentration. Fundamental studies have shown that aerated transient with air-saturated water can lead to non-reversible modification of oxides formed in nominal water [17], but its impact on SCC initiation in realistic operating conditions remains to be investigated. Some laboratory testing data is available on the effect of DO on SCC propagation in austenitic stainless steels, showing the presence of oxygen greatly accelerating the SCC crack growth rates of 304/316 in PWR primary water [18, 19]. However, similar evaluations are non-existent on the effect of DO on SCC initiation due to the known challenge in producing SCC initiation at constant load on Type 304/316 stainless steels in PWR primary water.

2.2 Key Knowledge and Technical Gaps

Based on the information collected on the operational experience of stainless steel SCC in PWR primary water and the literature review performed last year [3], high-quality SCC initiation data remains scarce to clarify the SCC initiation mechanism of Type 304/316 stainless steels in free-flowing PWR primary water. Existing laboratory data were mostly obtained using testing conditions far from realistic service conditions and cannot be directly used to inform proactive material degradation management. Key knowledge/technical gaps have been identified as follows:

- There is a lack of fundamental understanding of the factors responsible for SCC initiation and the development of very shallow surface cracks into deep propagating cracks. There is also a lack of quantifiable relationships between the influencing factors and SCC initiation time/susceptibility. For example, although field experience and literature data suggest cold work could accelerate SCC initiation, there is little information about threshold yield strength and hardness values required for SCC initiation in PWR primary water under free-flowing conditions. The same issues exist for dissolved oxygen content. The dependency of SCC initiation on temperature is largely unexplored. The contribution of creep to SCC initiation kinetics and mechanism is poorly understood. Heat-to-heat variability is another topic that may have been overlooked. In addition, the synergism between the influencing factors remains to be studied.
- There is a lack of suitable SCC initiation testing techniques that could effectively produce high-quality, reproducible SCC initiation data to be directly used to inform industry practice. At the same time, susceptibility map already exists for SCC propagation in PWR primary water [20] and for SCC initiation in BWR normal water chemistry [21]. Most of the existing body of SCC initiation data in PWR primary water is produced by SSRT using severe loading and excessive cold working that are difficult to relate to plant applications.

- There is a lack of statistically relevant SCC initiation data of austenitic SS in PWR primary water. Such data would be highly desired for industry to develop meaningful predictions on SCC initiation time/likelihood to guide inspection and maintenance strategy development.

2.3 Research Plan

To address these gaps, a research plan has been devised in FY 2024 based on updated information collected on the French NPP stainless steel auxiliary piping SCC experience and feedback from industry and the SCC research community. The objective of the research project is twofold: (1) To support the cause analysis of recent auxiliary piping SCC incidents reported in French NPPs focusing on knowledge gaps on environmental factors (i.e., dissolved oxygen and temperature); (2) To assess the potential relevance of the French NPP auxiliary piping SCC cases to the U.S. nuclear industry. Or, put in other words, to obtain a better mechanistic understanding of the conditions under which IGSCC could take place so that the industry and regulatory can be informed for guidance development as needed.

A general timeline of the research plan is provided in Table 2. It should be noted that the length of investigation for each task may be subject to minor changes depending on actual progress and results obtained. FY 2024 marks the first year of the research effort in this area with a focus on the evaluation of the effect of DO on SCC initiation of cold worked (CW) 304L in PWR primary water. The research progress made to date will be summarized in detail in the following chapters.

Table 2. PNNL's research plan on SCC initiation testing of stainless steels in PWR primary water.

Research Task	FY24	FY25	FY26	FY27	FY28
Effect of DO on SCC initiation of cold worked 304L					
Effect of DO on SCC initiation of cold worked 316L					
Acquisition of weld mock-up with high weld residual stress					
Effect of DO on SCC initiation of non-aged weld mock-ups					
Aging of weld mock-ups & characterization					
Effect of temperature on SCC initiation of cold worked 304L*					
Effect of temperature on SCC initiation of cold worked 316L*					
Effect of temperature on SCC initiation of non-aged weld mock-ups*					
SCC initiation testing of aged weld mock-ups (scope and timeline to be defined in future based on results obtained from above tasks)					

*Tasks will continue into FY29.

3. Materials Information

3.1 Heat Selection

The typical grades for auxiliary stainless steel in the U.S. fleet are 304, 304L, 316, and 316L. A survey of PWROG fleet of 55 units found no cases of 316LN grades being used [22]. To assess the potential relevance of French NPP auxiliary piping SCC incidents to U.S. nuclear industry, 304L and 316L were selected as testing materials for this study. One heat was purchased each for a dual-certified 304/304L and 316/316L (denoted as 304L and 316L hereafter) in the plate form with a thickness of 6.35 mm (2.5 inches). This thickness was selected to enable 0.5”-thick compact tension specimens being extracted in the S-L, S-T, L-S, and T-S orientations as shown in Figure 9 after being forged up to 50% reduction in thickness, which is likely needed to produce materials with high hardness matching the threshold of 300 HV reported for SCC to occur in service in non-contaminated PWR primary water [8].

Certified mill test reports were obtained on multiple heats for selection, and the final choice was made based on a balance of desired composition (higher carbon, higher nitrogen, lower sulfur, lower molybdenum, and lower copper) and mechanical properties (higher strength) that are known to increase SCC susceptibility. The basic information and composition of the two purchased heats are listed in Tables 3 and 4, respectively.

Table 3. Basic materials information of the purchased 304L and 316L heats.

Material	Heat No.	Form	Heat treatment condition	Yield Strength at Room Temperature (MPa)
304/304L	530059	2.5” thick plate	Solution annealed at 1050°C and quenched in water	295
316/316L	Y35Y	2.5” thick plate	Solution annealed at 1038°C and quenched in water	272

Table 4. Chemical composition of the purchased 304L and 316L heats.

Heat # / Weight (wt%)	530059 (304/304L)	Y35Y (316/316L)
C	0.017	0.021
Si	0.32	0.423
Mn	1.2	1.187
P	0.031	0.033
S	0.001	0.001
Cr	18.23	16.600
Ni	8.02	10.035
Mo	0.56	2.017
Cu	0.38	0.431
N	0.07	0.056
Co	-	0.275

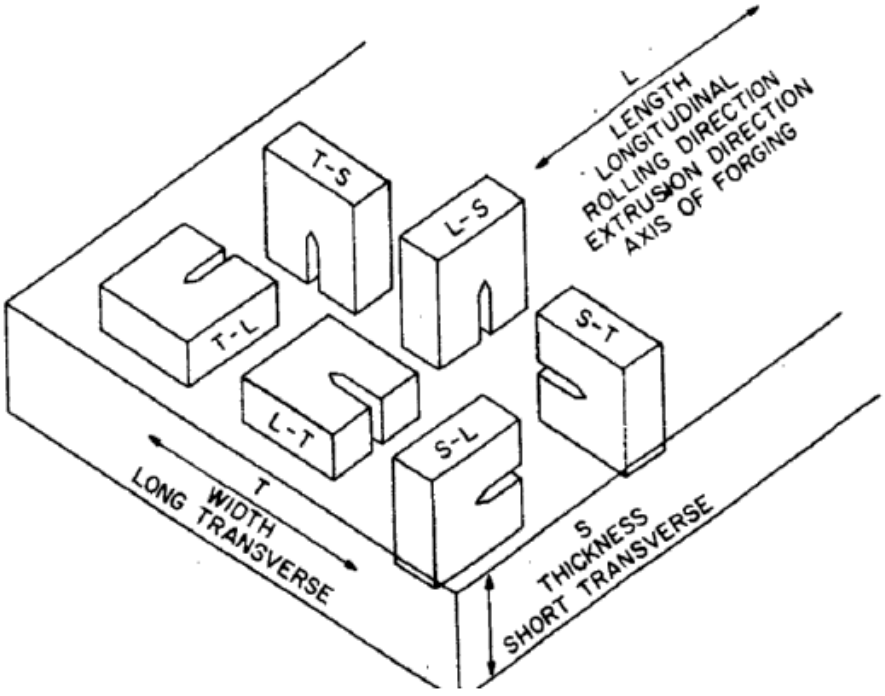

Figure 9. Specimen orientation for a plate product form [23].

3.2 Cold Forging Procedure

To evaluate the effect of cold work on materials' SCC initiation susceptibility, and to produce materials that match the high hardness values (~300 HV) reported on SS components where SCC incidents were detected in service, it was decided to cold forge the 304L and 316L materials to various

cold work levels for this study. While the microstructures produced by cold forging may not be fully representative of that of the HAZ in an actual weld, it provided a cost-effective way to identify the appropriate combination of oxygen content, loading conditions, and strain paths to produce SCC initiation in SS materials in a realistic time frame, which is also a critical goal of the first phase of this study.

As shown in Figure 10, four blocks of ~ L3.5" × W3" × T2.5" were prepared for 304L and 316L to be cold forged to 10%, 20%, 30%, and 40% reduction in thickness. The blocks to be cold forged to 30% and 40% reduction in thickness were further cut into half to facilitate the forging. The cold forging was performed at General Electric Global Research Center (GEGRC). To avoid strain-induced martensite formation during cold forging, the blocks were preheated in a furnace for several hours or overnight to reach a uniform temperature of ~210°C. To achieve this, the blocks were placed on an alumina base, which was linked to a thermal couple. The temperature on the thermal couple only varied from 207–210°C over the entire preheating duration. The forging was conducted immediately after the blocks were removed from the furnace. A photo of the post-forged 304L blocks is provided in Figure 11.

The FY 2024 testing effort focused on 304L. For the first series of tests, four blunt notch compact tension (BNCT) specimens and two cylindrical tensile specimens were machined from the 304L blocks in each cold forged condition. The tensile specimens were prepared for tensile testing to obtain yield strength (YS) of these cold forged materials at 300°C (i.e., SCC initiation testing temperature). The BNCT specimens were prepared for SCC initiation testing. The reason behind the selection of this geometry for testing will be discussed later in Section 4.1.1. As shown in Figure 12, the tensile and BNCT specimens were all prepared in the L-S orientation for the first phase testing because this orientation is coincident with the cracking path in actual welds in auxiliary stainless steel piping in the French PWRs.

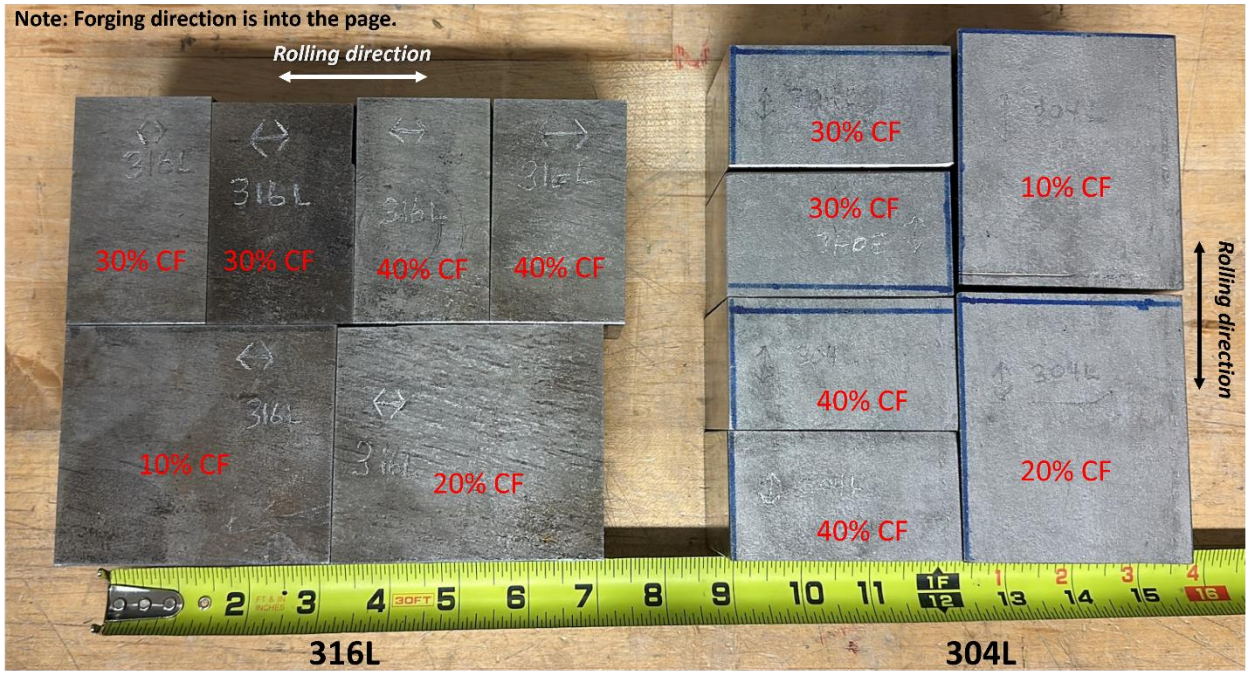

Figure 10. 304L and 316L blocks prepared for cold forging.

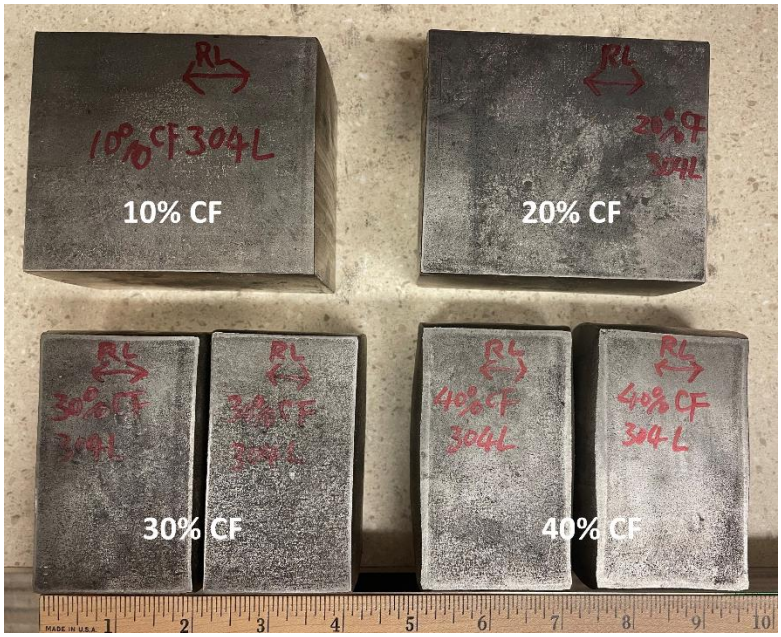

Figure 11. 304L blocks after being cold forged to 10–40% reduction in thickness. The forging direction is into the page.

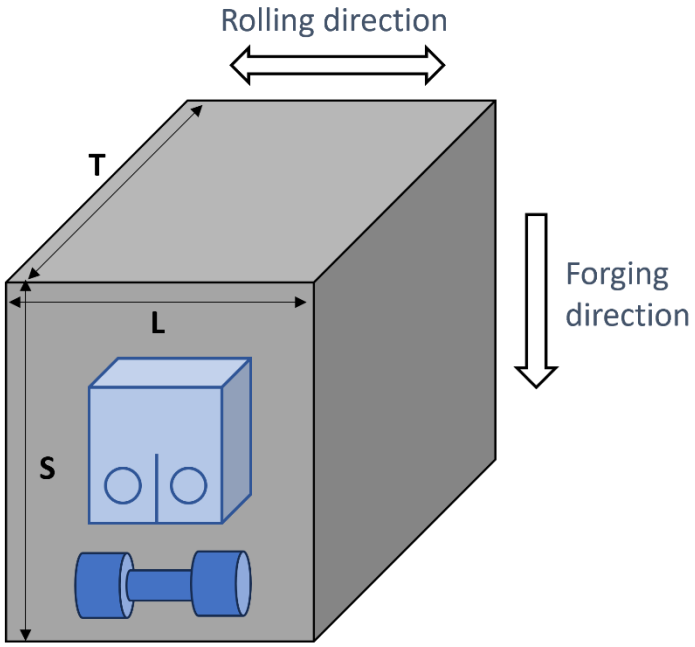

Figure 12. Schematic showing the specimen orientation with respect to the rolling direction of the as-received 304L and 316L plate materials and the direction of forging performed at GEGRC. L = longitudinal, T = transverse, and S = short transverse.

3.3 Characterizations of Cold Forged 304L

After the materials were cold forged, a ≥1/3-inch thick piece was taken off from one end of a block at each cold forged level and cut into three smaller samples for microstructural characterizations and hardness measurements. The LS, TS, and TL planes of the forged blocks were all sampled as indicated by the different colors in Figure 13a. The three samples from the same cold forged block were then mounted together in an epoxy base (Figure 13b) and prepared through standard metallographic procedures beginning with grinding using SiC pads of 220-1000 grit, followed by 6 µm and 1 µm diamond paste and 0.05 µm colloidal silica vibratory polish for high resolution microscopy characterizations.

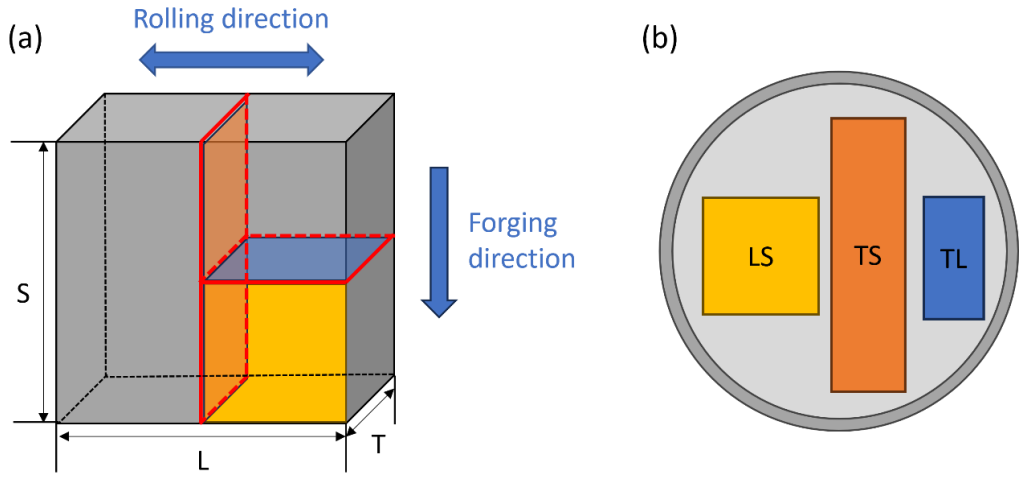

Figure 13. Schematic showing (a) the cutting plan of three samples from materials at each cold forged level and (b) their corresponding polishing plane in the epoxy mount.

3.3.1 General Microstructures

As the first step, a JEOL 7600F field emission scanning electron microscope (SEM) was used to document the materials microstructures at each cold forged level in both secondary electron (SE) and backscattered electron (BSE) modes. Figure 14 displays the general microstructure observed in the 10, 20, 30, and 40% CF 304L materials, respectively. Strain contrast induced by cold work was observable and quantitative analysis results will be shown in Section 3.3.3. Randomly distributed darker stringers of 25–100 µm long are visible in all CF levels at similar densities, which are confirmed as delta ferrites in the following electron dispersive spectroscopy (EDS) and electron backscatter diffraction (EBSD) analyses.

High resolution examination found that there were often some micrometer- and sub-micrometer-sized, irregularly shaped secondary phase particles residing on the matrix-delta ferrite interfaces (Figure 15). Cracked precipitates and adjacent voids were also visible by the brighter edges revealed in these SE mode images (as highlighted by the red arrows). These damages are likely produced by cold forging and they share similar morphologies as those previously reported in thermally treated and cold forged Alloy 690 materials [24]. While no quantitative analysis was performed, these observations indicate that the degree of damage increases with the cold forge level, which is qualitatively demonstrated in these images. It is possible that these damages can act as stress concentrators, and there may be galvanic effects between the precipitates, delta ferrite, and matrix that can facilitate crack initiation at such sites. However, the density of these precipitates thus associated damage is very low, therefore unlikely to cause macroscopic SCC initiation even in the 40% CF specimens. Nevertheless, their impact on SCC initiation can only be confirmed by post-test examinations, and we will aim to obtain unambiguous evidence to prove/disprove the hypothesis. In addition, increasing strains with the increase in cold forge level can also be viewed more clearly in these higher-magnification images.

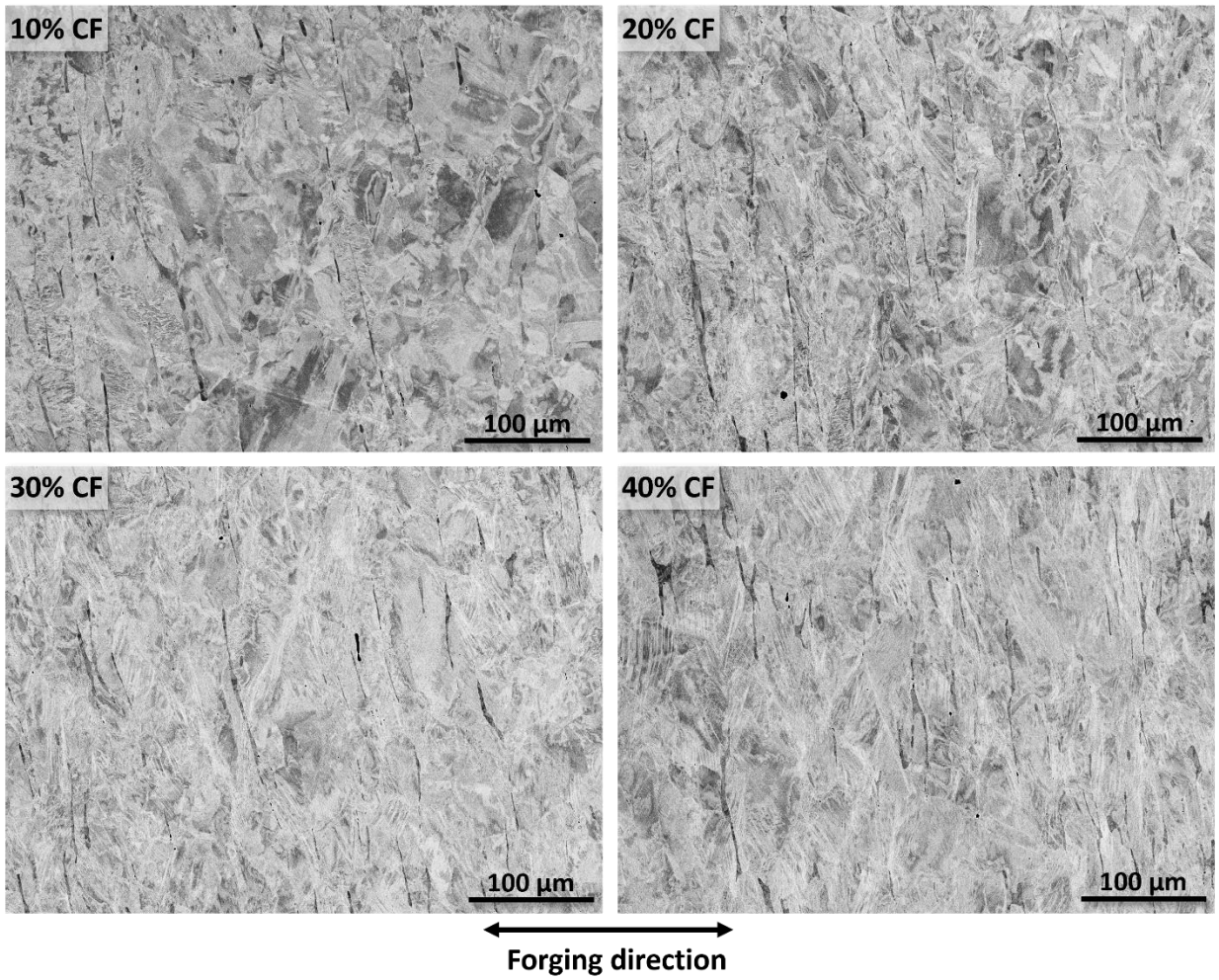

Figure 14. Representative SEM-BSE images of the microstructure in the TS plane of 304L cold forged to 10–40 % reduction in thickness.

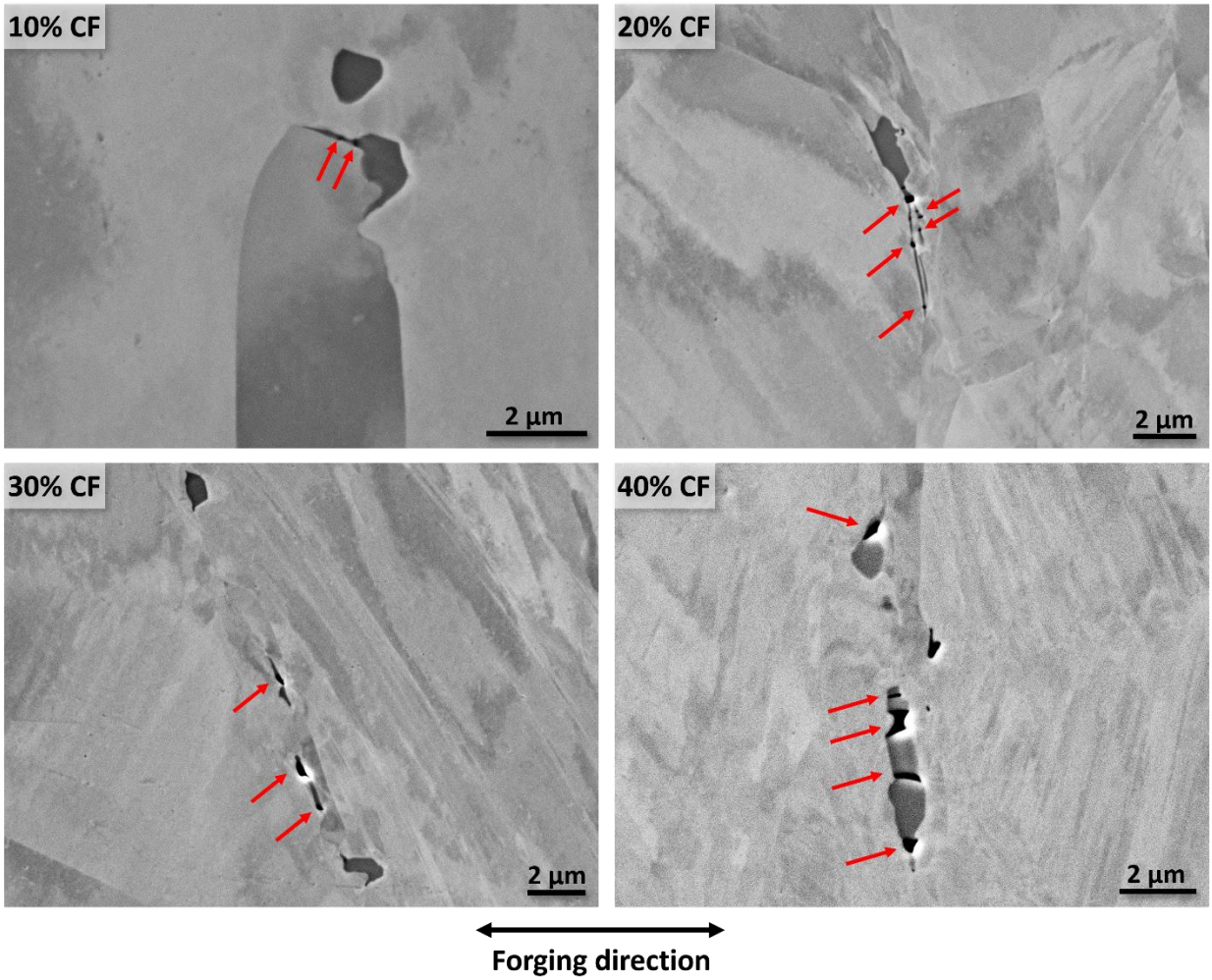

Figure 15. SEM-SE images of representative precipitates and cold forge-induced damage in the TS plane of the 10–40%CF 304L materials. Voids or cracks in precipitates produced by cold forging are highlighted with red arrows.

3.3.2 EDS Analysis

SEM-EDS analyses was performed first at low magnifications to obtain the general chemical composition of randomly selected sites in each cold forge level using a voltage of 20 keV. Figure 16 shows an example with selected elemental maps of an area documented in the TS plane in the 40%CF 304L material. The darker stringers revealed in the BSE image are high in Cr and low in Ni content, consistent with delta ferrite characteristics. In addition, enrichment of Cr, Al, and Ti were observed at certain spots, indicating secondary phases of different types.

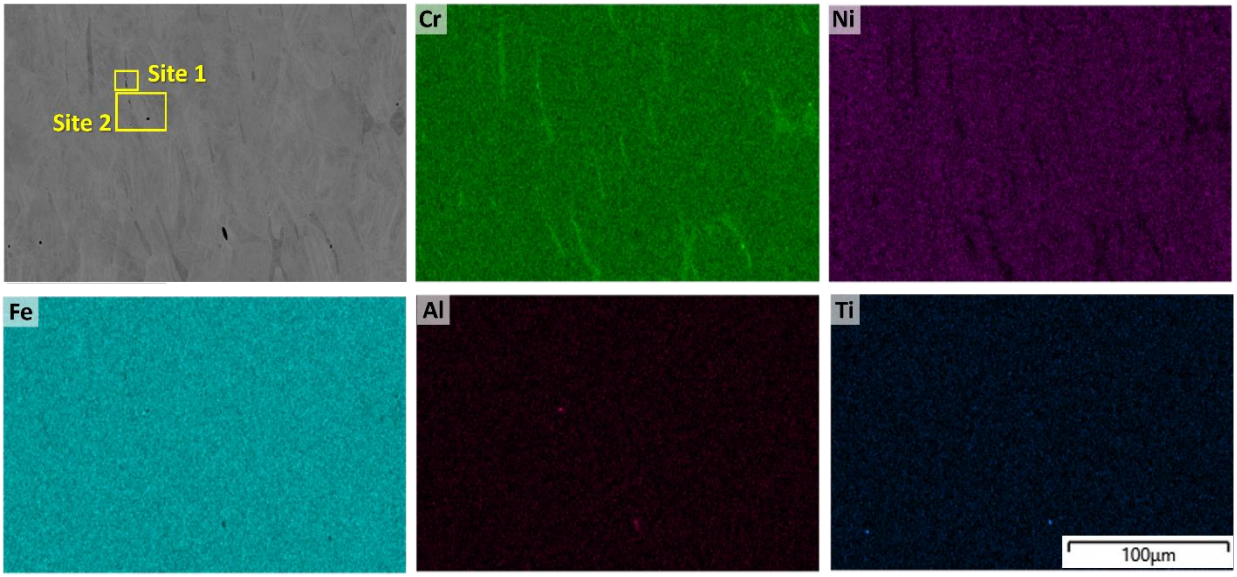

Figure 16. SEM-EDS elemental mapping of the general microstructure in the 40%CF 304L material (TS plane view).

SEM-EDS analyses were then performed at higher magnifications focusing on obtaining chemical composition information on different types of secondary phases revealed in the low magnification maps. A lower voltage (10 keV) was used, taking advantage of the smaller interactive volume of the beam to obtain more accurate data on the precipitates found on the surface and on lighter elements. The results of the EDS analysis performed on the two sites selected in Figure 16 are shown in Figures 17 and 18, respectively. Site one features a few Cr-rich precipitates residing on the left side of a delta ferrite, where enrichment of silicon is found in the cracks in the lower precipitate, consistent with the colloidal silica suspension used at the final step of polishing. The irregularly shaped, darker, sub-micrometer-sized secondary phase residing on the right side of the delta ferrite features a more complex composition with Ti enriched in the needle-like strip immediately adjacent to the delta ferrite, while enrichment of Mn, S, and Al is found to the right of the Ti-enrichment in the lower rod-like portion, indicating a mix of titanium nitride and manganese sulfide inclusions. Site 2 also exhibits a few Cr-rich precipitates residing on the left side of a delta ferrite and an intragranular inclusion to the right of the delta ferrite. Figure 18 suggests this is a much bigger titanium aluminum nitride with titanium-rich outskirt wrapping an Al- and N-rich core.

Observations on 304L materials at other cold forged levels agree with the above findings. It can thus be summarized that at least three types of secondary phases are present in the 304L materials: Cr-rich precipitates, MnS inclusions, and TiN inclusions. The Cr-rich precipitates usually reside at the delta ferrite-matrix interfaces, while TiN have been observed at the delta ferrite-matrix interfaces and in the matrix. Since only one MnS was found by the limited EDS analyses performed, it is not possible to determine whether it has a favorable nucleation site. Since MnS is known to deteriorate the corrosion resistance of stainless steels and promote pitting especially in chloride-containing waters, it will be of interest to see if they can act as crack initiation site in oxygenated PWR primary water. More detailed examinations will be performed post-test to determine the extent of MnS distribution and their effects on SCC initiation of stainless steels.

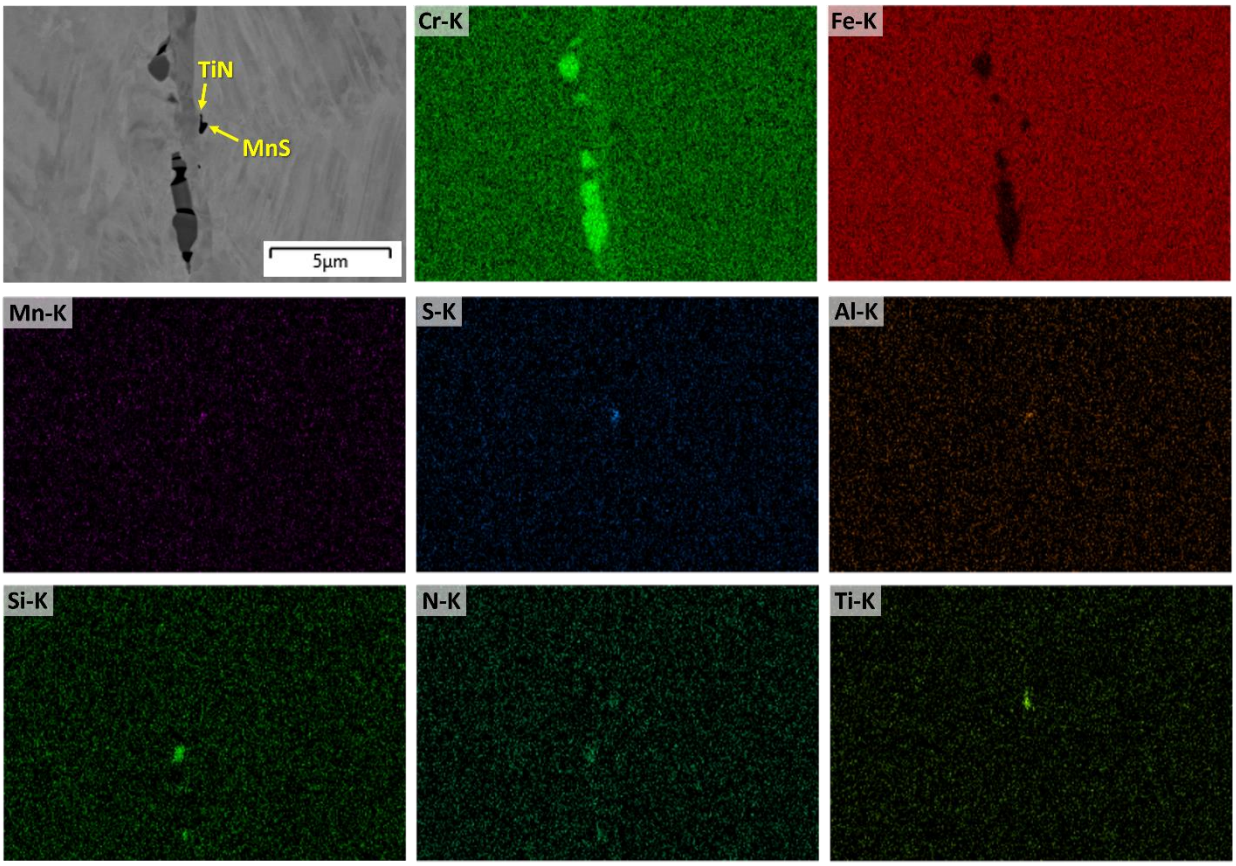

Figure 17. Qualitative SEM-EDS elemental mapping of precipitates found at Site 1 as highlighted in Figure 16 in the 40%CF 304L material.

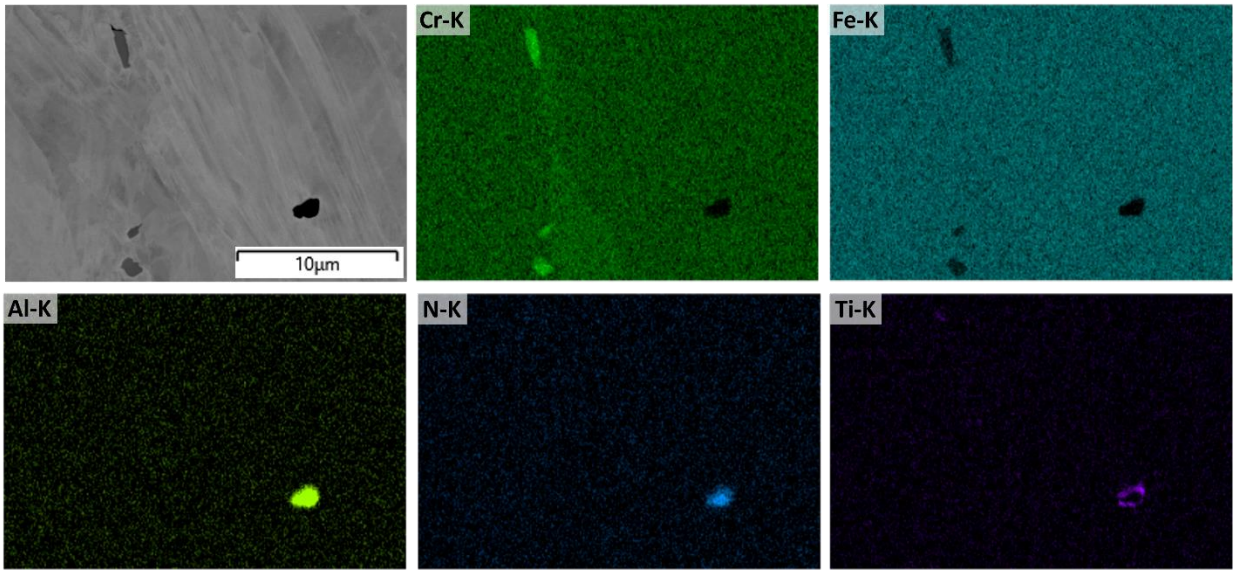

Figure 18. Qualitative SEM-EDS elemental mapping of precipitates found at Site 2 as highlighted in Figure 16 in the 40%CF 304L material.

3.3.3 EBSD Analysis

EBSD was performed to obtain crystallographic information of the cold forged blocks with a focus on the distribution of phases, local misorientations, and grain boundary types. A JEOL-IT800 FESEM equipped with an Oxford Instruments Symmetry detector was used. The imaging condition was 20 KeV at ~70° tilt and a working distance of ~25 mm. The EBSD focused on the middle sample shown in Figure 13b, i.e., the TS plane sample, of each cold forge level. Analysis was performed at four different magnifications, namely 100X, 250X, 400X and 2500X, using step sizes of 1 µm, 0.5 µm, 0.15 µm and 20 nm, respectively. Data cleanup was conducted using the Oxford's AZtecCrystal v3.1 software, first to remove mis-indexed electron backscatter patterns and then to perform an iterative zero solution extrapolation to a medium level. For highly strained samples (40% CF), additional data cleanup was done utilizing spherical harmonic indexing (MapSweeper) of diffraction patterns for particularly weak intensities. This allows for an increase in data for analysis and adequate comparison between the different forging levels.

Figures 19–22 summarize the inverse pole figures, phase maps, kernel average misorientation (KAM) maps, and grain boundary type maps obtained at 400X magnification on the TS plane of 304L cold forged to 10, 20, 30, and 40% reduction in thickness, respectively. These maps provided information on the general microstructure of materials cold forged to the four different levels. The increase in cold forging level has led to an obvious decrease in grain size (Figure 19) and increase in local misorientation (Figure 21). The local misorientation mostly concentrated near grain boundaries in all cold forge conditions, while increased deformation inside grains were observed in highly CF materials, especially in the 40%CF condition. A small fraction of twin boundaries, mostly $\sum 3$ type boundaries, were seen through materials with different cold forge levels without obvious variation in density (Figure 22). Delta ferrites are present in materials in all cold forged conditions and their shape were obviously impacted by cold forging, with a trend of becoming narrower along the plane perpendicular to the forging direction and more fragmented as the forging level increases. The comparison of the phase maps and grain boundary type maps indicates that while some delta ferrites are present inside the grains, a much higher proportion is adjacent to high angle grain boundaries. Higher magnification EBSD maps were acquired at 2500X with refined step size and the results are summarized in Figure 23. The primary goal of these examinations is to confirm that martensite does not exist in these cold forged materials, as expected given the preheating conducted on these materials right before forging. The martensite phases were included for indexing, but the 10 and 20%CF showed no trace of these phases. In some of the higher CF samples, there were hints of some martensite phase near grain boundaries, but the data was sparse and not quantifiable. As a result, it can be concluded that the preheating performed before forging successfully prevented martensite from forming during cold forging. Even if martensite exists, they only occasionally present at discrete sites and, therefore, will have negligible impact on materials' mechanical properties and SCC resistance.

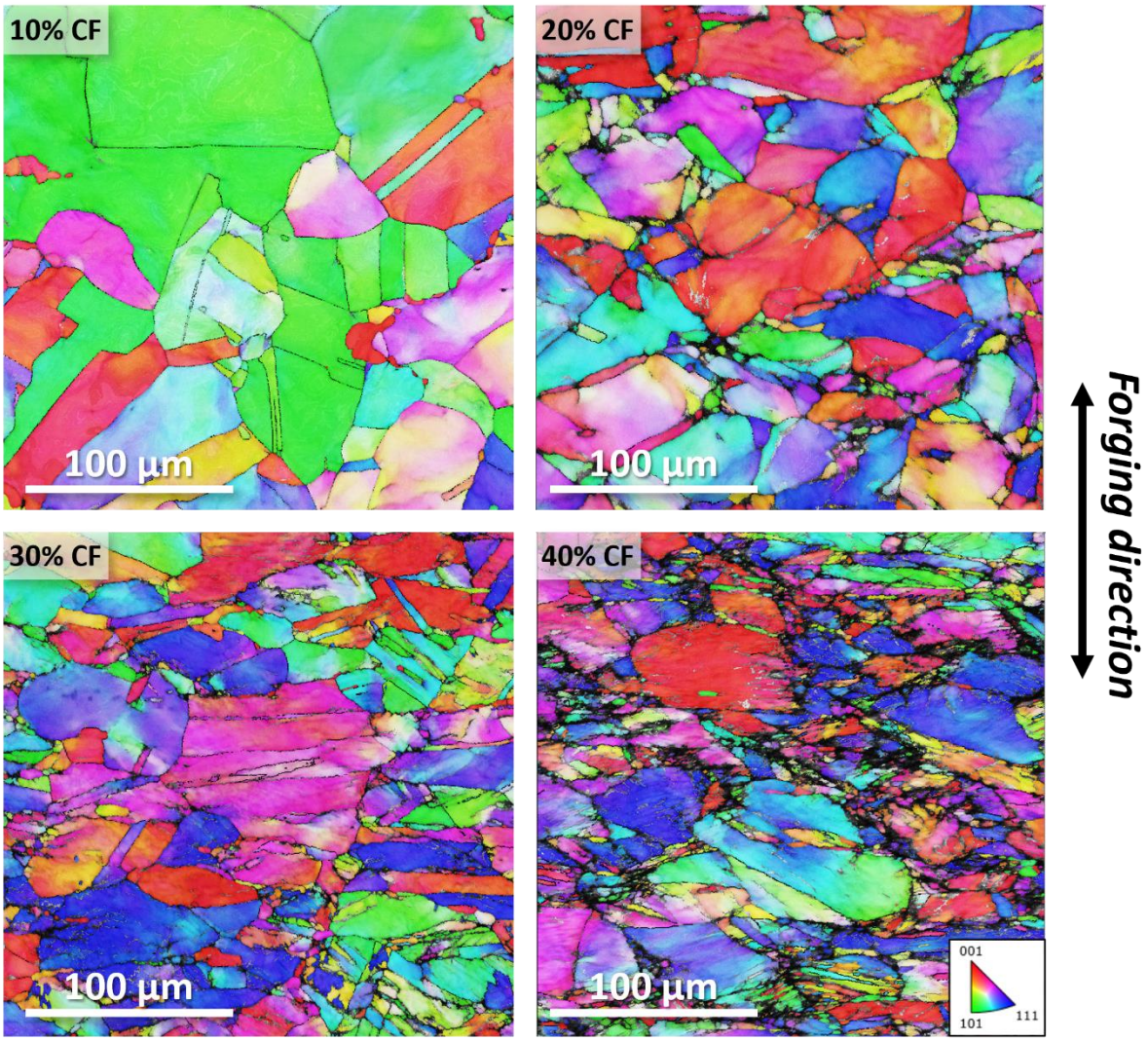

Figure 19. Comparison of EBSD inverse pole figures of the 10, 20, 30, and 40%CF 304L materials. Images were all taken at 400X from the TS plane.

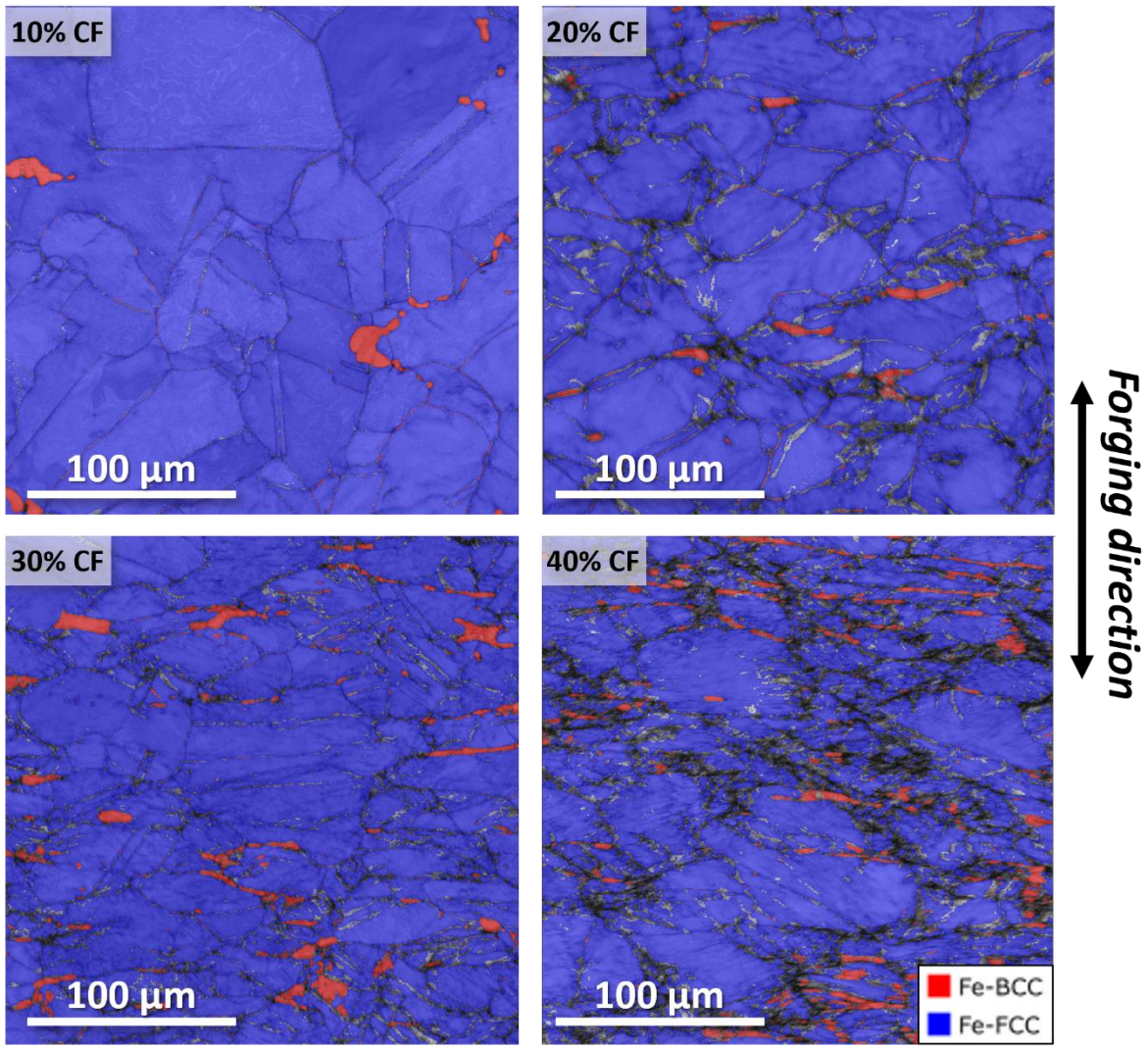

Figure 20. Comparison of EBSD phase maps of the 10, 20, 30, and 40%CF 304L materials. Images were all taken at 400X from the TS plane.

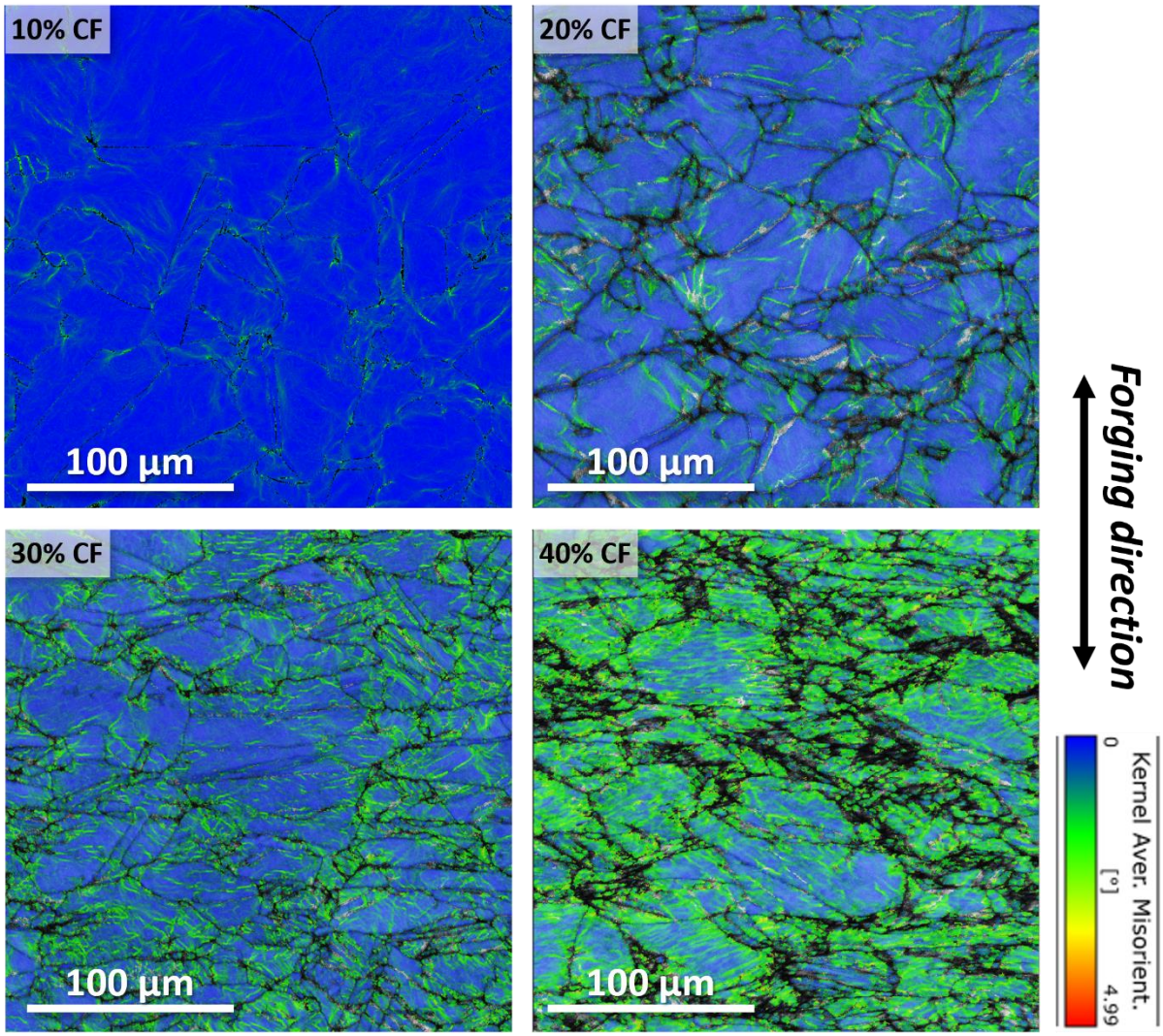

Figure 21. Comparison of EBSD local misorientation (KAM) maps of the 10, 20, 30, and 40%CF 304L materials. Images were all taken at 400X from the TS plane.

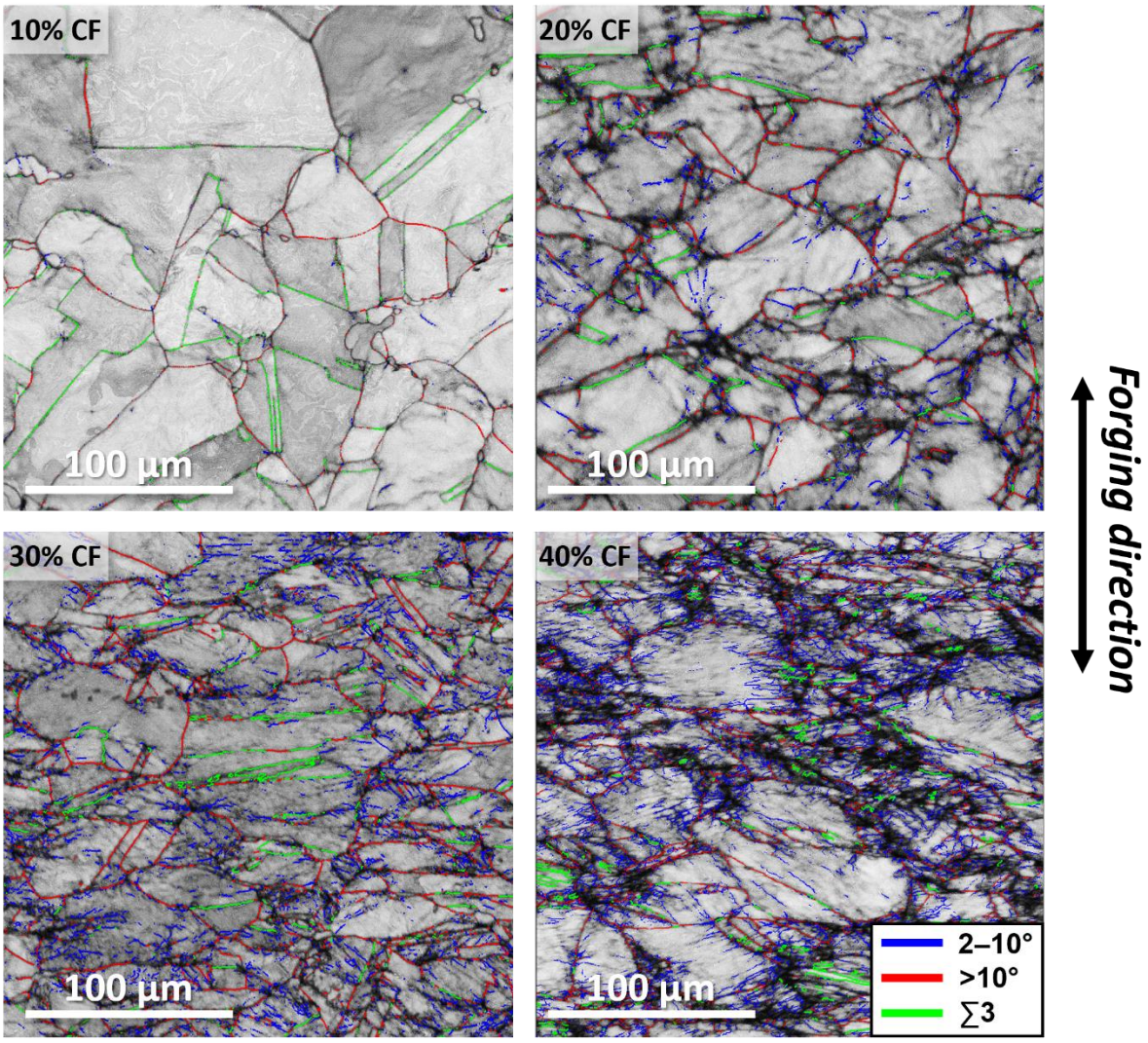

Figure 22. Comparison of EBSD band contrast and grain boundary type maps of the 10, 20, 30, and 40%CF 304L materials. Images were all taken at 400X from the TS plane.

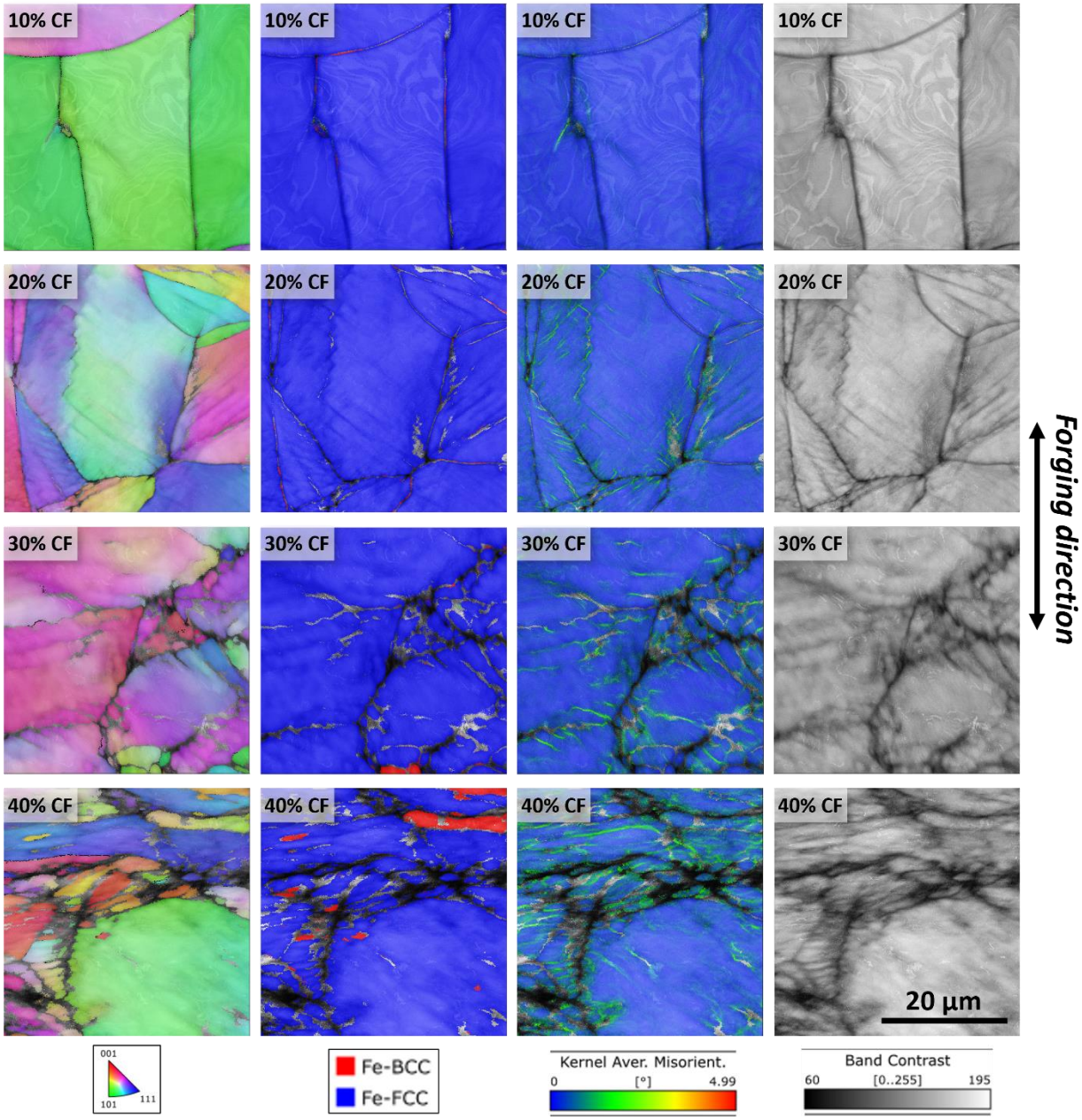

Figure 23. Comparison of EBSD maps taken at 2500X on the TS plane of the 10, 20, 30, and 40%CF 304L materials. Columns from left to right are inverse pole figures, phase maps, KAM maps, and band contrast maps, respectively.

3.3.4 Hardness Measurements

After the completion of all SEM characterizations, microhardness measurements were performed on these mounted samples. For each CF condition, all three samples prepared from different planes of the cold forged block as shown in Figure 13b were measured. A Series CM-802 Micro Indentation Clark Instrument was used with a load of 300 gf and a dwelling time of 12 seconds per indent. As shown in Figure 24, the sampling area is a ~3×3 mm^2 region at the center of each specimen, which includes ~120 indent points.

The measured average hardness data is summarized in Table 5 and plotted in Figure 25 for better visualization. The average hardness values measured from each plane steadily increased with increasing cold work, and the difference in hardness values among the planes are within statistical error at each cold forge level. As shown in Table 5, the overall average hardness measured for the 10%CF 304L material is ~224 HV, and increased by 30 HV to 255 HV for the 20%CF material. Then the increase in hardness slowed down and increased by 15HV for each 10% additional increment in cold forging level, resulting in an average hardness value of ~288 HV for the 40%CF 304L material. This trend is best interpreted by a power law fit as shown in Figure 26, which suggests that 50%CF level is required to reach an overall average hardness of ~300 HV, consistent with what was reported in literature [8].

Nevertheless, it should be noted that the scatter in hardness values increased with increasing cold work, which is expected since the cold work induced more local inhomogeneity. Figure 27 provides an example on the hardness fluctuation measured on each plane of the 40%CF 304L material. Regions of hardness values exceeding 300 HV interweaved with regions with hardness values as low as 220 HV, showcasing the inhomogeneous nature of hardness distribution. From the standpoint of this study, the cold forging conducted on 304L has successfully produced high hardness values matching those measured on French SS auxiliary piping where SCC incidents were reported (Figures 03 and 04), and will be used for subsequent SCC initiation testing.

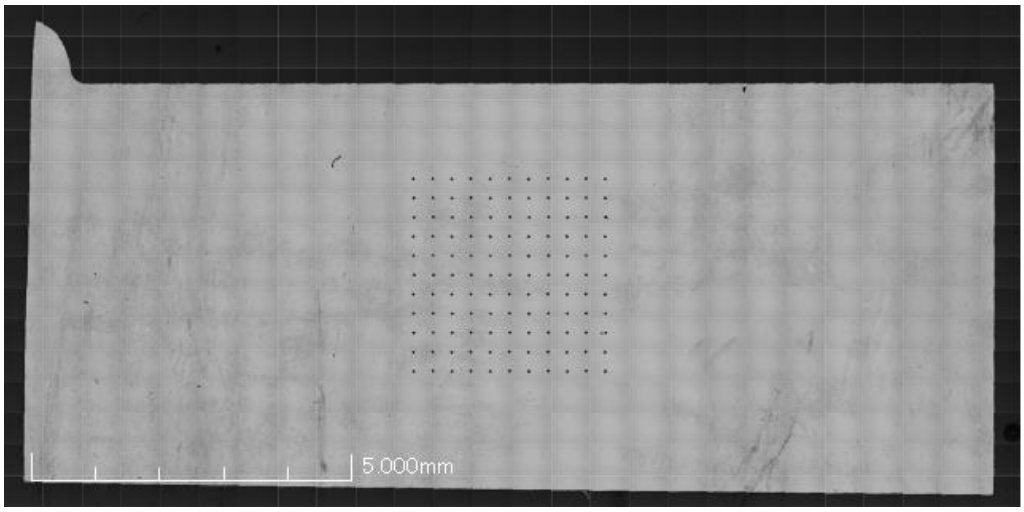

Figure 24. An optical micrograph showing the typical area sampled for hardness measurement in the specimens.

Table 5. Measured hardness values for the cold forged 304L materials.

Hardness / Material	Avg. HV (kg/mm^2)			
	LS plane	**TS plane**	**TL plane**	**All planes**
10% CF 304L	228.7±7.2	221.7±8.4	222.7±8	224.4±8.4
20% CF 304L	258.2±10.1	253.6±11.5	253.0±9.9	254.9±10.8
30% CF 304L	276.2±16.9	252.9±15.2	272.0±11.4	270.4±15.7
40% CF 304L	282.8±25.7	294.3±14.7	285.4±17.9	287.5±20.5

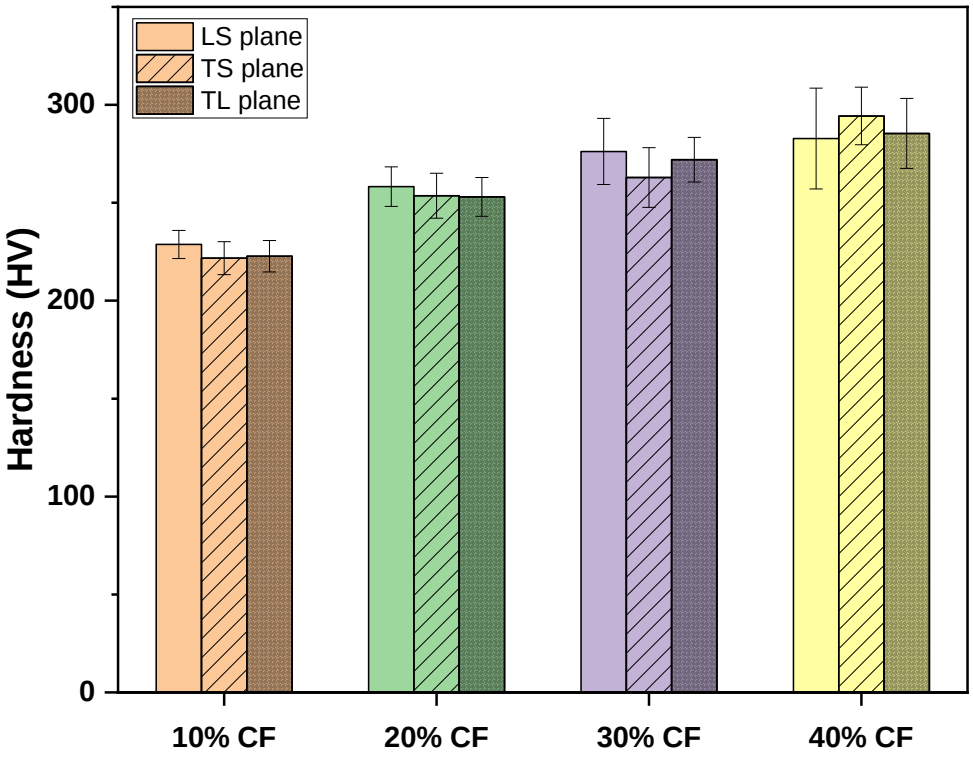

Figure 25. Hardness values measured on the LS, TS, and TL planes of the 304L blocks cold forged to 10%, 20%, 30%, and 40% reduction in thickness.

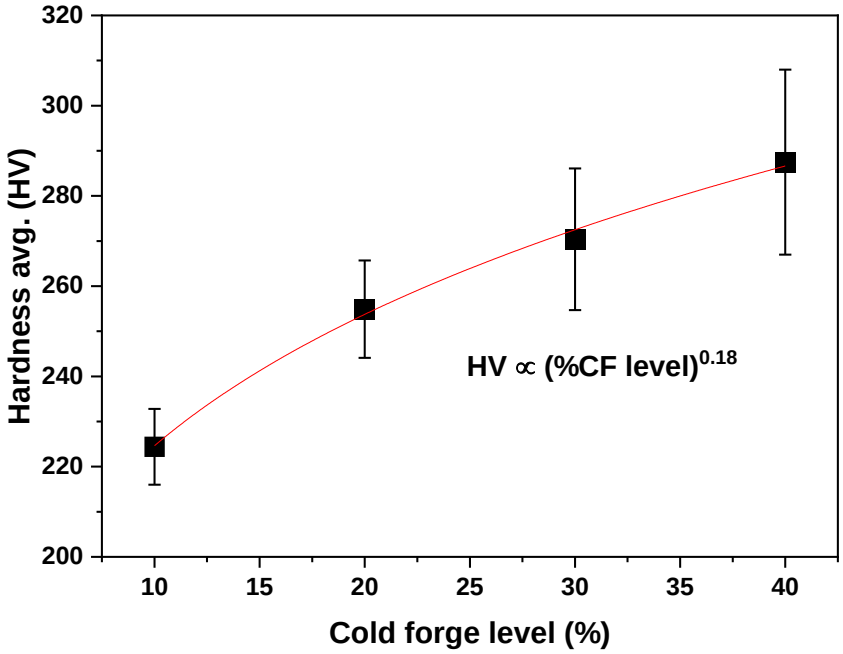

Figure 26. Overall average hardness values as a function of cold forge level.

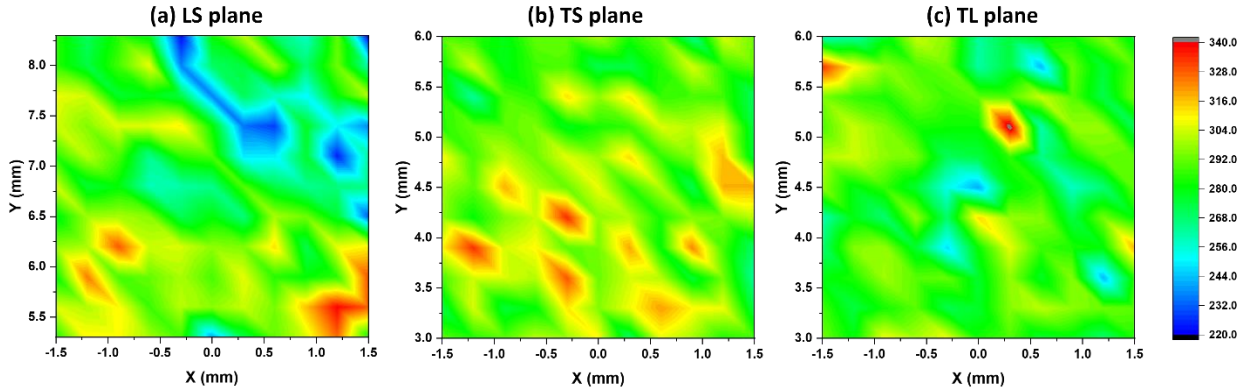

Figure 27. Hardness contour maps on the three planes of the 40%CF 304L material.

3.3.5 Tensile Testing

Tensile properties were measured on materials cold forged to all four levels. The orientation and dimensions of the tensile specimens used for this testing have been shown in Figures 12 and 28, respectively. The testing temperature was set at 300°C, the same temperature at which the SCC initiation testing will be performed. The stress vs. strain curve for all four cold forged condition is shown in Figure 29. Since the primary objective was to obtain the YS of these materials, the tests did not continue till specimen failure, but were stopped after a few percentages of plastic strain were reached after yielding. The obtained YS values are plotted against the corresponding hardness data of the same material and summarized in Figure 30. They were correlated with both the hardness values measured from the TS plane, i.e., the plane normal to the loading direction of the tensile specimens, and the overall averaged hardness values measured from all three planes. A very similar linear dependence was found between the hardness values and material's YS in the form of $hardness = A \times YS$, where A varied between 0.28 and 0.30.

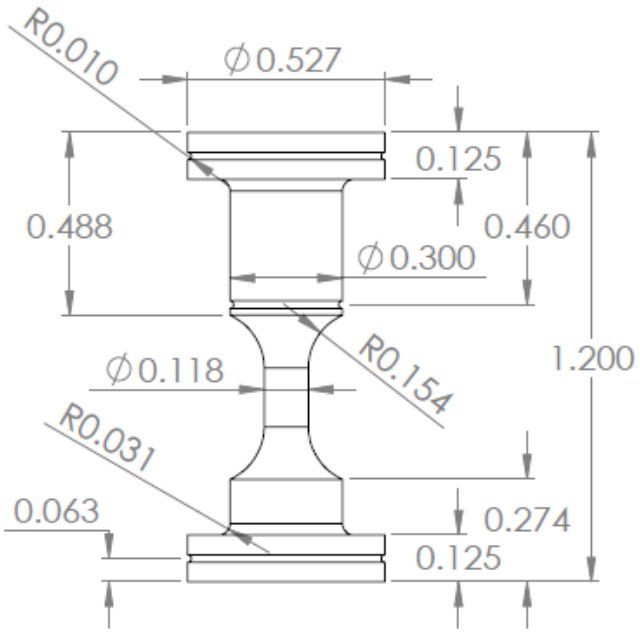

Figure 28. Dimensions of the tensile specimens (unit: inch).

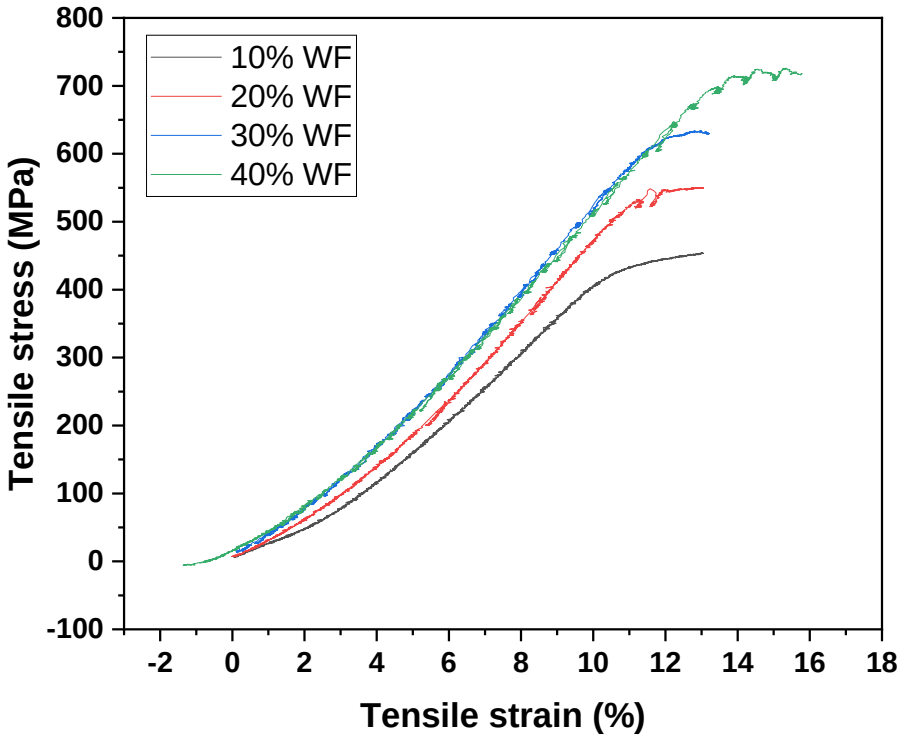

Figure 29. Stress vs. strain curve for the 10–40%CF 304L materials obtained in 300°C air.

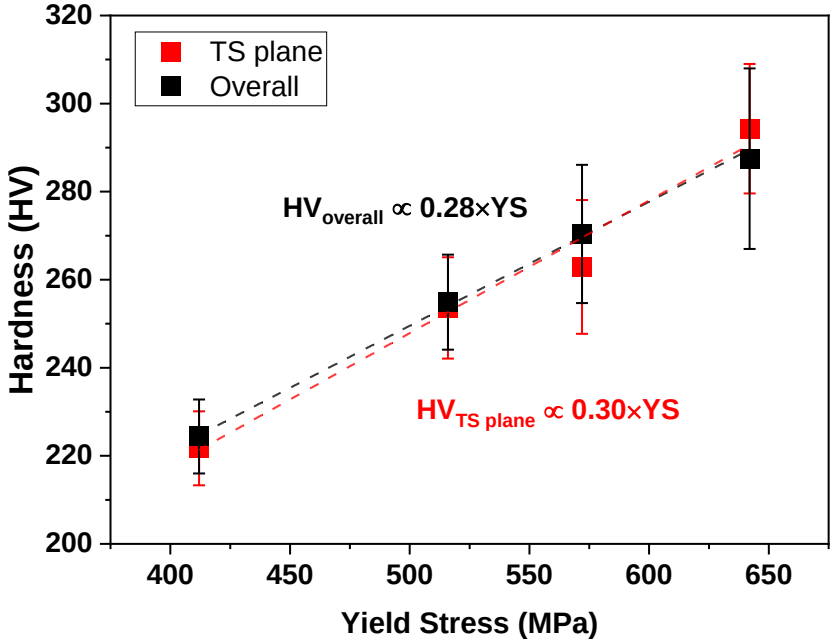

Figure 30. Hardness measured on the TS plane and the overall average hardness measured from all three planes in the 10–40%CF 304L materials as a function of their yield stress.

4. Test Update

4.1 Experimental

4.1.1 Specimen Preparation

A general consensus summarized in our previous literature review [3] is that traditional constant load tensile specimen SCC initiation tests on 304L/316L may not be able to produce crack initiation, even in a highly cold worked condition. Complex strain paths and/or some amount of strain cycling appears to be necessary in promoting SCC initiation. BNCT specimen offers the flexibility to incorporate these two factors in the initiation testing. Its geometry allows for multi-axial loading at the notch bottom. It also enables strain cycling and enhanced deformation in the high stress region near the notch bottom without risking the specimen to fail due to transitioning to instability like what can happen with tensile specimens. As a result, the BNCT specimen geometry was chosen for the first phase SCC initiation testing of CF 304L.

Standard 0.5T CT specimens with dimensions shown in Figure 31 were machined using electrical discharge machining (EDM). As illustrated in Figure 12, all specimens were extracted in the L-S orientation so that the cracking plane aligns with the crack growth direction in actual circumferential welds in the auxiliary piping. To remove the EDM recast layer and to allow documentation of crack initiation sites, the notch surface was manually polished to a 1 μm finish using special tools developed in house. Before the start of the test, SEM examinations were performed to confirm quality of polish on the notch surface. As shown in Figure 32 shows examples of acceptable surface finish on the notch bottom of the BNCT specimens. Although some polishing marks still remain due to the challenging geometry for polishing, the delta ferrites were clearly revealed with clean edges. Some strain contrasts were also visible on the notch surface. If the polish did not reach such degree, the specimens will be returned for more polishing until an acceptable quality was confirmed via iterative SEM examinations.

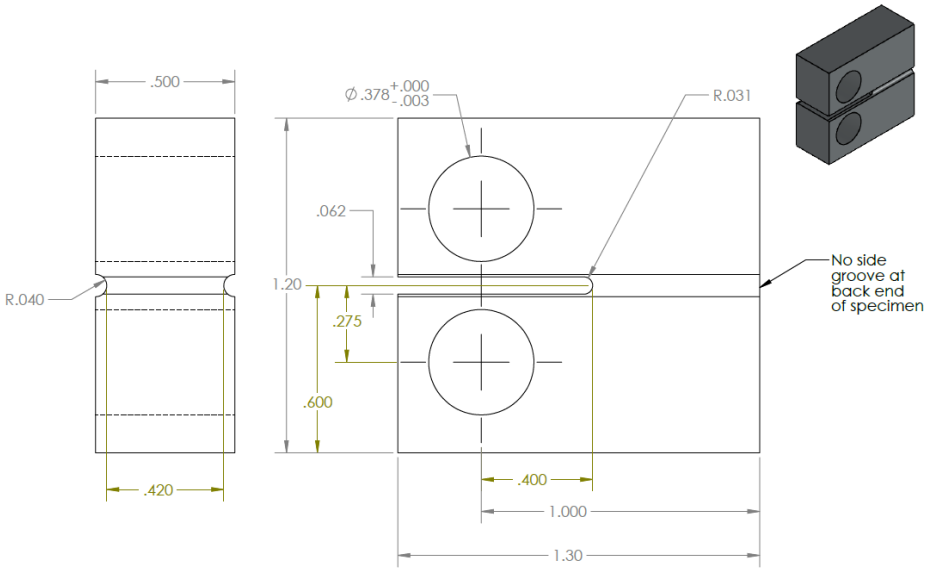

Figure 31. Dimensions of the blunt notch CT specimens (unit: inch).

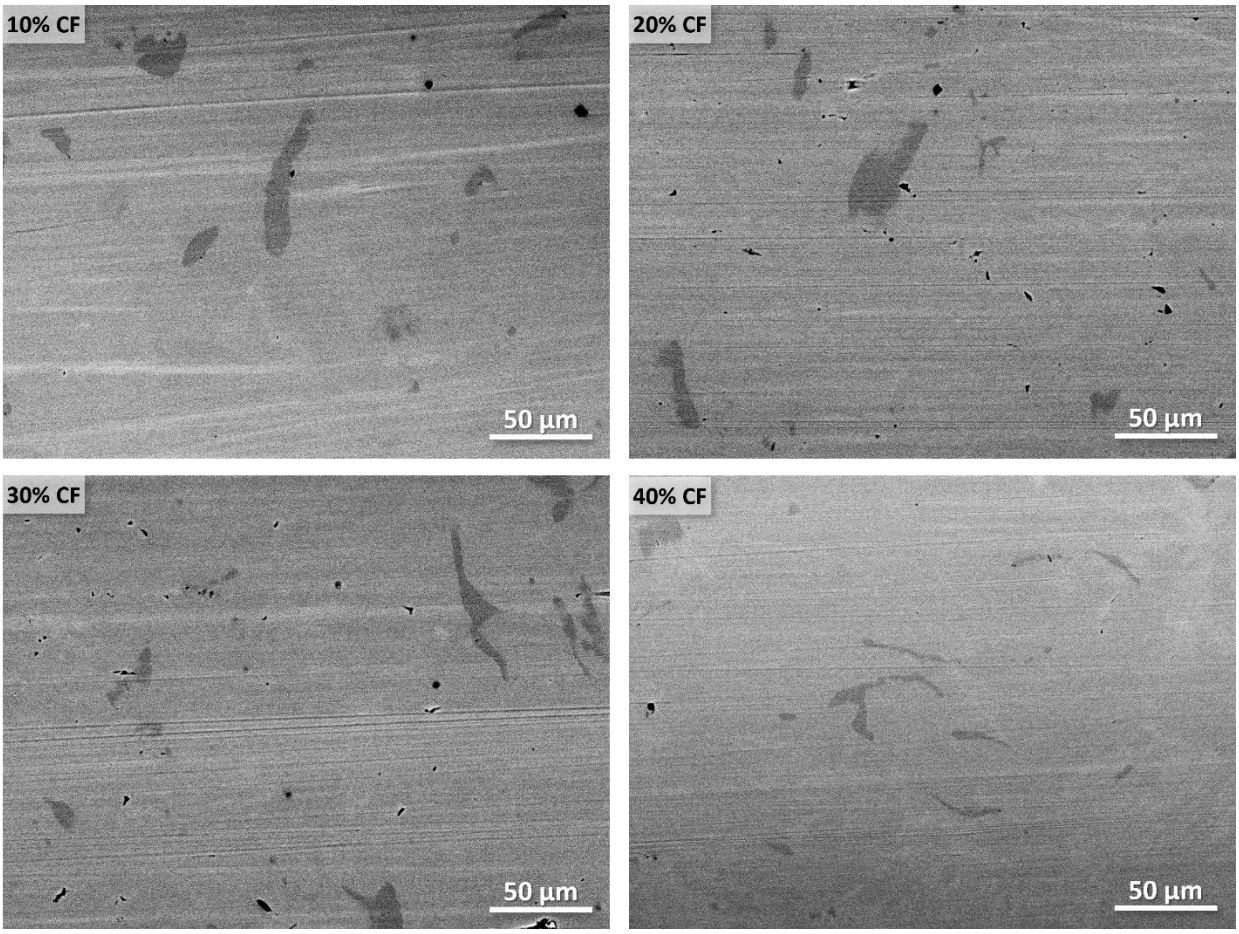

Figure 32. SEM-BSE images on typical morphology of the polished surface on the front face of the notch bottom.

4.1.2 SCC Initiation Testing

The two mid-sized LWRS SCC test systems (denoted as LWRS2 and LWRS3 hereafter) are being used for the first phase testing. The SCC test systems are equipped with active load control via a high-precision servo-electric load control system and in-situ monitoring using direct current potential drop (DCPD) technique. Detailed information on the development of the SCC test system and DCPD technique can be found in previous publications [25]. As shown in Figure 33, four BNCT specimens (one from each cold forging condition) are loaded in series in each test systems. The test environment simulates PWR primary water with 1000 ppm of boron and 2 ppm of lithium at 300°C, the highest operating temperature reported for the SS auxiliary piping.

4.1.2.1 Oxygen Content Selection and Control

As discussed in Section 2.1, it is very challenging to determine the level of DO representative of the values that may be present in SS auxiliary piping. While performing discontinuous oxygen ingress in hydrogenated water better simulates the actual environment the auxiliary stainless steel piping may be exposed to in the French PWRs, it was decided to focus on constant DO levels as the first step to screen the effect of DO on SCC initiation. After discussing with the industry and reviewing literature data, two DO levels were chosen for the first test in the two test systems: 2 ppm DO in LWRS2, and 50 ppb DO in LWRS3 to screen the effect of DO on SCC initiation of 304L. A number of SCC crack growth rate and

low cycle fatigue studies on 304L/316L used these same DO contents for testing, allowing future comparison to be made with our SCC initiation testing results if applicable. It is hypothesized that SCC initiation will occur faster in the CW 304L materials in the primary water with 2 ppm DO than with 50 ppb DO, so another test will be started in LWRS2 with a medium DO content (e.g., 200 or 500 ppb DO) after the 2 ppm DO test is completed. However, this plan will be reviewed and revised if needed depending on the actual testing result of the first two tests.

During the test, the DO content was maintained at the preset value via running an oxygen feeding tube to the water column of each test system. Mixed oxygen-nitrogen gas bottles with specific volume ratios were purchased and fitted with a 0-60 PSI regulator that was set to 15 PSI to ensure a steady flow out from the bottle. The tubing from the regulator to the water column gas inlet was then attached to an isolating valve in line with a metering valve. Once all connections were made, the lines were flushed of any potential residual gases before the test was started. The metering valve was then set at the calculated pressure needed to achieve the desired DO content in each test system. The combination of using the metering valve with a pressure regulator on the water column allows a steady pressure to be maintained on the oxygen feed thus constant DO content during testing. In addition, the outlet conductivity of the flow loop is being continuously monitored during testing, providing an indicator on the stability of the DO level in the test system.

Figure 33. The loading train with four BNCT specimens installed and spot welded with insulated Pt wires for in-situ DCPD monitoring of crack initiation and growth.

4.2 Current Status

4.2.1 SCC Initiation Test in PWR Primary Water with 2 ppm DO

This test was started at constant load with a stress intensity (*K*) of ~30 MPa√m for four BNCT specimens CT304-307, one each from the 10, 20, 30, and 40% CF condition. These *K* levels are better described as a "pseudo *K*" as they are calculated assuming a tight crack is present across the specimen versus a blunt notch with a smooth surface. The *K* of 30 MPa√m was chosen as it has been commonly used for SCC crack growth rate testing of cold worked stainless steels, and is considered as a reasonable start point for the SCC initiation test.

The test was started in early July 2024 and an overview of the DCPD-indicated crack length evolution from the notch of the four tested specimens is shown in Figure 34. The trend for all specimens during the first 800 hours of testing are generally flat or slightly negative, which should be phantom and is likely associated with internal strain redistribution under loading and the oxides formation on the notch surface. Since many studies in literature pointed out that constant load may not be sufficient to induce SCC initiation in 304L/316L even in highly cold worked conditions, it was decided to stop the test after reaching 800 hours of exposure to examine the notch surface of all specimens for precursor damage and initiation indications. The results are summarized in Figures 35–38 for the 10%, 20%, 30%, and 40%CF specimen, respectively. Although not obvious in these low-magnification images, formation of surface oxides was confirmed on the notch surface of all specimens. No prominent evidence of intergranular corrosion was observed in any of these specimens. It is worth noting that a high density of slip bands were identified on the notch surface of the 10% and 20%CF 304L specimens, with examples shown in the lower images in Figures 35–36. In comparison, no slip bands were observed in the 30% and 40%CF 304L specimens (Figures 37–38). These observations suggest that the constant load at 30 MPa√m had led to substantial localized hardening in the notch region of the 10% and 20%CF 304L specimens but to a much less degree in the 30% and 40%CF 304L specimens, which is consistent with the lower YS measured for the 10% and 20%CF 304L materials (Section 3.3.5). Was et al. [26] has long been suggesting that dislocation channels, presented in the form of stacked slip planes, has a key role in irradiation assisted SCC initiation in austenitic stainless steels. When encountering a grain boundary (GB), the dislocation channels (DC) can either transfer to a neighboring grain (i.e., continuous DC) or terminate at the grain boundary (i.e., discontinuous DC), resulting in very different strain/stress states at the DC-GB site. The discontinuous DC-GB site exhibit a much higher stress and has been shown to lead to a much higher probability of cracking than that for continuous DC-GB sites. In addition, it has been reported that a high propensity for crack initiation was seen when discontinuous dislocation channels intersect MnS inclusions in 304L [27]. Since MnS inclusion has been confirmed in the 304L being tested in this study, it would also be of interest to evaluate the interactions between DO level, precipitates, and loading condition to obtain a better understanding of SCC initiation mechanism in these CF 304L materials when applicable.

As the immediate next step, it was decided to increase the constant load from 30 to 40 MPa√m on all specimens during the subsequent testing and monitor the DCPD response for at least 1,000 more hours. Another test interruption is planned after that and future testing conditions will be determined based on the next-round SEM examination results. Currently, the four BNCT specimens CT304-307 have been reinstalled in LWRS2 in preparation for the test restart.

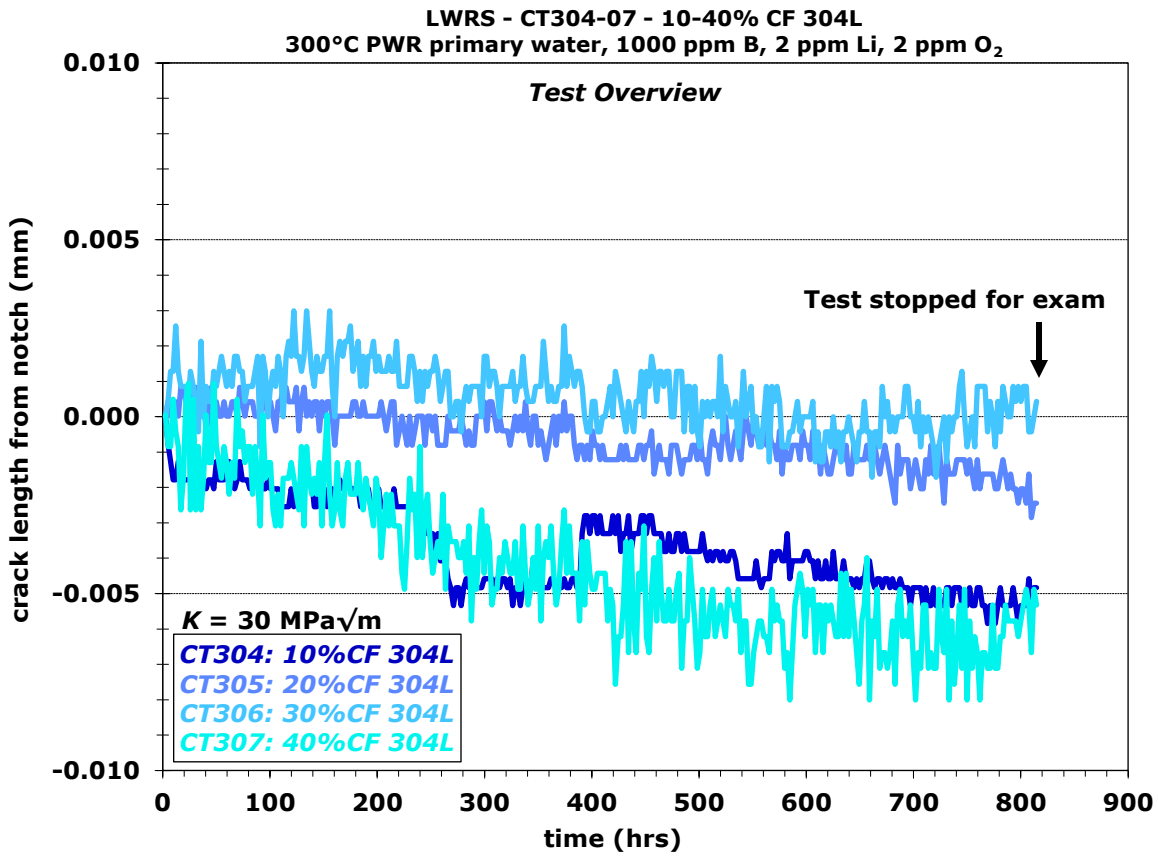

Figure 34. Test overview of the crack length evolution in 10–40% CF 304L BNCT specimens in 300°C PWR primary water containing 2 ppm DO.

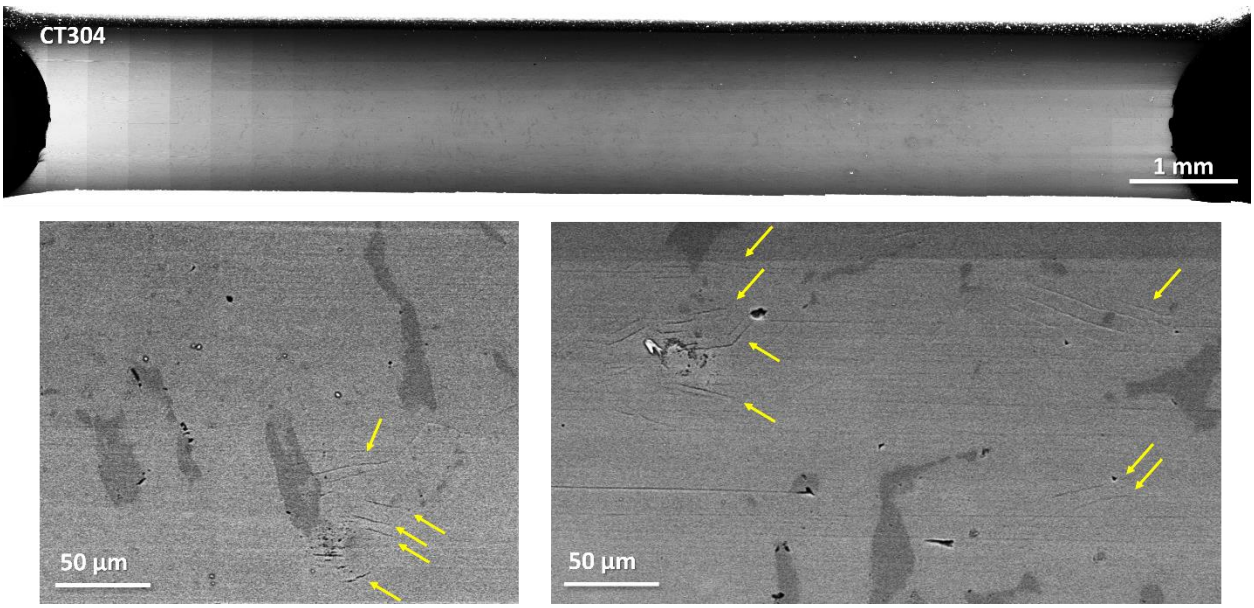

Figure 35. SEM-BSE montage image (upper) of the notch surface of the 10%CF 304L BNCT specimen CT304 after 815 hours of exposure in 300°C PWR primary water containing 2 ppm DO, with higher

magnification images at randomly selected sites on the notch surface (lower). Observed slip bands are highlighted by arrows.

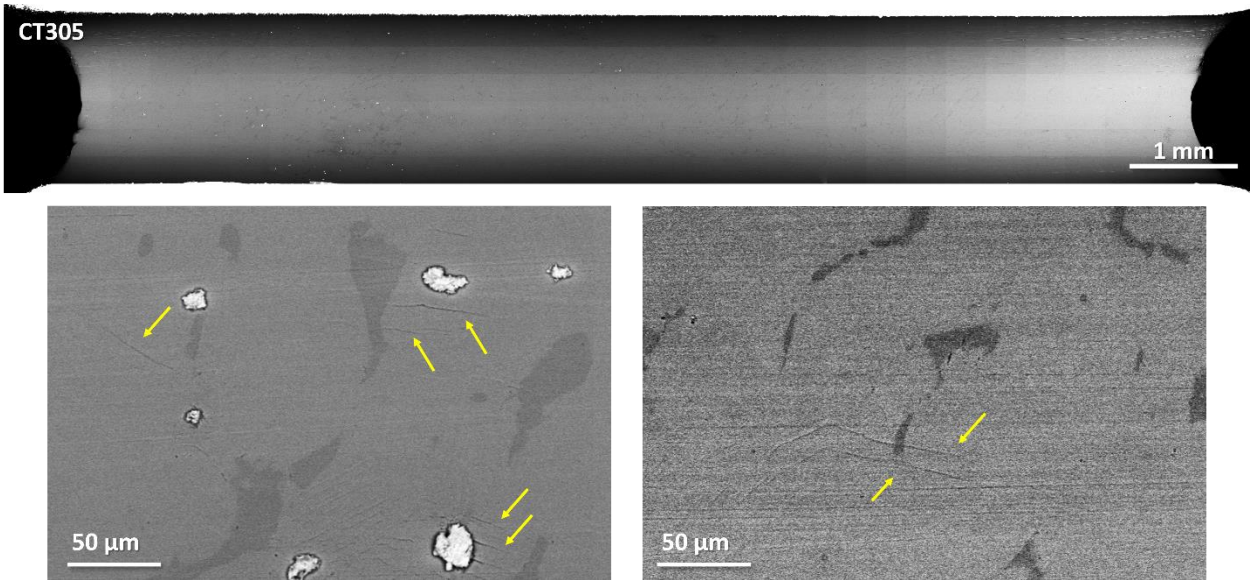

Figure 36. SEM-BSE montage image (upper) of the notch surface of the 20%CF 304L BNCT specimen CT305 after ~815 hours of exposure in 300°C PWR primary water containing 2 ppm DO, with higher magnification images at randomly selected sites on the notch surface (lower). Observed slip bands are highlighted by arrows.

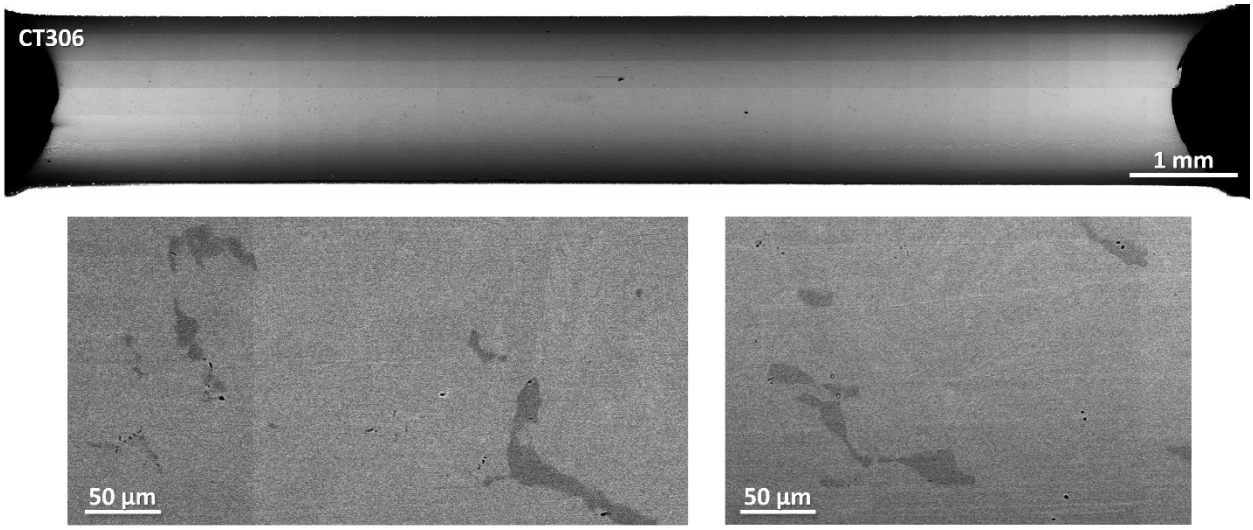

Figure 37. SEM-BSE montage image (upper) of the notch surface of the 30%CF 304L BNCT specimen CT306 after ~815 hours of exposure in 300°C PWR primary water containing 2 ppm DO, with higher magnification images at randomly selected sites on the notch surface (lower).

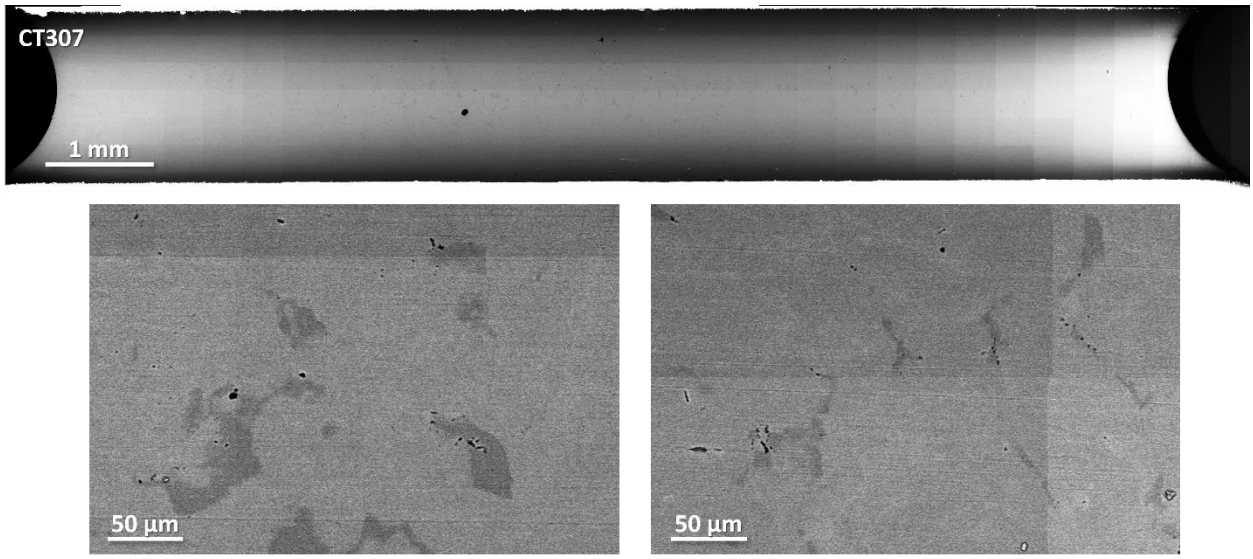

Figure 38. SEM-BSE montage image (upper) of the notch surface of the 40%CF 304L BNCT specimen CT307 after ~815 hours of exposure in 300°C PWR primary water containing 2 ppm DO, with higher magnification images at randomly selected sites on the notch surface (lower).

4.2.2 SCC Initiation Test in PWR Primary Water with 50 ppb DO

This test was started in August 2024 at the same loading condition as the test with 2 ppm DO on another set of four CF 304L specimens CT308–311, one each from the 10%, 20%, 30%, and 40% CF condition. The DO content of this test is maintained at 50 ppb. A constant load at a "pseudo *K*" of ~30 MPa√m is applied on all the specimens. The test overview of the DCPD-indicated crack length evolution from the notch of the four tested specimens is provided in Figure 39. The test currently reached a similar total exposure time (~860 hours) as the test in LWRS2, showing a generally flat or slightly negative slope in crack length evolution for all specimens. This suggests that no obvious crack initiation has yet occurred in any of the specimens. Since the notch surface morphology of the specimens likely are very similar to those observed in CT304–307, no test interruption is planned at the moment to stop the test for notch surface examinations. It has been decided to increase the constant load from 30 to 40 MPa√m together with the test in LWRS2 and monitor the crack length evolution for at least another 1,000 hours. After that, the specimens will be taken out for detailed notch surface examination to devise the testing plan for subsequent exposure.

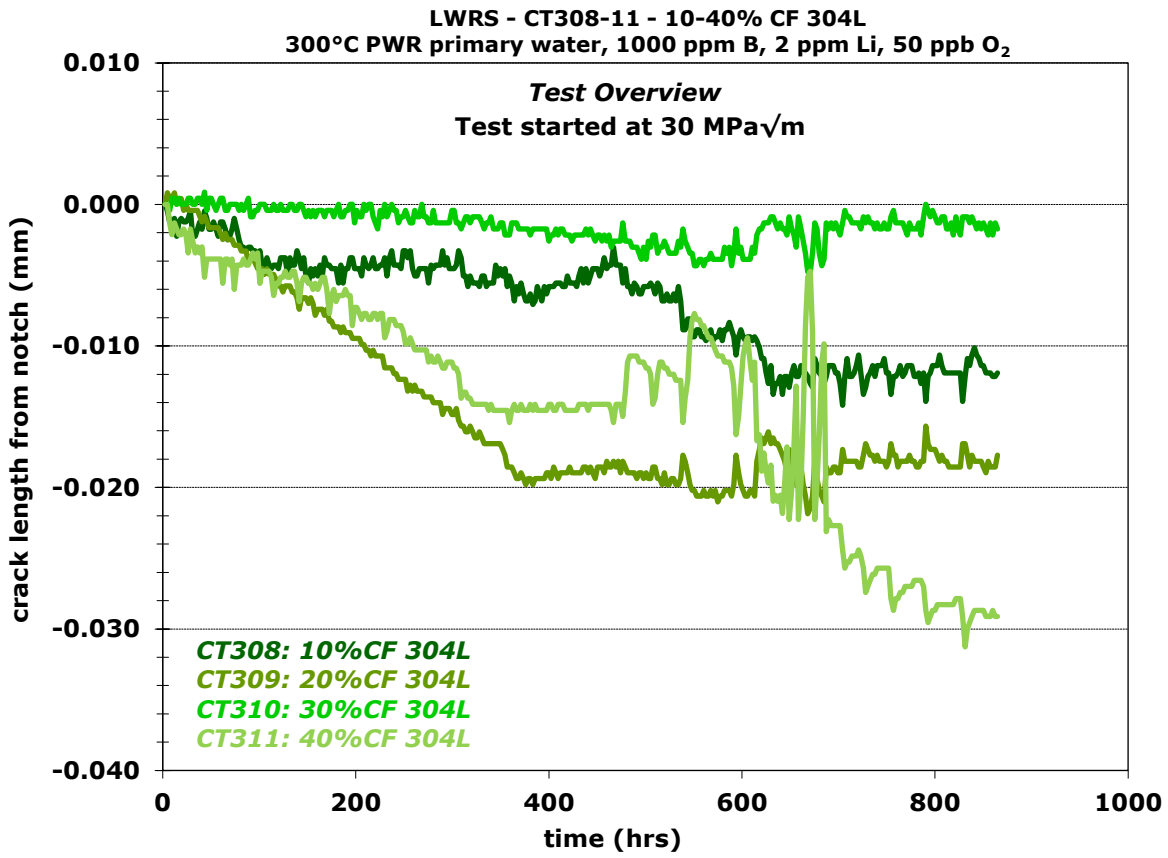

Figure 39. Test overview of the crack length evolution in 10–40% CF 304L BNCT specimens in 300°C PWR primary water containing 2 ppm O_2.

5. Summary

The IGSCC cases recently reported in 304L/316L(N) auxiliary piping weldments in multiple French PWRs demonstrated that austenitic stainless steels are not immune to IGSCC in free-flowing, non-contaminated primary water. These SCC incidents were among the first cases reported in non-isolable portions of branch piping in the PWR primary circuit, posing threat to nuclear safety and have led to significant financial loss. While weld residual stress has been considered to play a key role in these incidents, it is also recognized that high residual stress alone is insufficient in causing the magnitude of IGSCC cases detected to date. The SCC initiation mechanisms remain largely convoluted due to the complex welding history, operating conditions, and metallurgical characteristics, requiring more systematic studies to determine the effect of each key influencing factor and their interactions. The current study is established to address this need with two primary objectives. The first is to support the cause analysis of recent auxiliary piping SCC incidents reported in French NPPs focusing on knowledge gaps on environmental factors (i.e., dissolved oxygen and temperature). The second goal is to assess the potential relevance of the French NPP auxiliary piping SCC cases to the U.S. nuclear industry. Or, put in other words, to obtain a better mechanistic understanding of the conditions under which SCC can initiate and grow, so that the industry and regulatory can be informed for guidance development as needed. In this report, the research activities carried out on this study in FY 2024 are summarized. Commercial 304L and 316L materials were purchased and cold forged to 10%, 20%, 30%, and 40% reduction in thickness. Detailed characterizations including SEM examinations, hardness measurements, and mechanical testing were completed for the 10–40% cold forged 304L materials. Key microstructural, crystallographic, and compositional information and mechanical properties were documented to facilitate testing plan finalization and/or to be correlated with specimen SCC initiation response later on. Two constant load SCC initiation tests have begun on 10–40% cold forged 304L BNCT specimens in 300°C PWR primary water containing either 2 ppm DO or 50 ppb DO. The crack extension response of all specimens is being monitored in-situ by DCPD for crack initiation detection. To date, both tests have accumulated 800+ hours of exposure at an estimated stress intensity of 30 MPa√m with no DCPD indication of SCC initiation in any of the specimens. Work hardening evidenced by slip bands has been observed on the notch surface of the 10% and 20% CF 304L specimens, but not in the 30% and 40% CF 304L specimens after 800 hours of testing in 2 ppm DO-containing PWR primary water. It has been decided to increase the constant load from 30 to 40 MPa√m for both tests to see if SCC initiation can be detected in realistic testing durations before adding cyclic loading to further accelerate SCC initiation. The tests are currently ongoing and new results will be reported in the future.

REFERENCE

[1] G. O. Ilevbare, F. Cattant and N. K. Peat, "SCC of stainless steels under PWR service conditions", in Fontevraud 7 - 7th International Symposium on Contribution of Materials Investigations and Operating Experience to LWRs' Safety, Performance and Reliability, 2011, France.

[2] R. Hosler, "Auxilliary Piping SCC OE Focus Group Update (Industry Perspectives), in Advisory Committeee on Reactor Safeguards (ACRS) Meeting 11/16/2022 on French PWR Safety Injection System Cracking ". November 2022.

[3] Preparation for Stress Corrosion Crack Initiation Testing of Austenitic Stainless Steels in PWR Primary Water. Pacific Northwest National Laboratory: Technical Milestone Report M3LW-23OR0402039, Light Water Reactor Sustainability Program, DOE Office of Nuclear Energy, June 2023.

[4] Nouvelles détections de fissures sur des tuyauteries du système d'injection de sécurité des réacteurs n° 1 et n° 2 de la centrale nucléaire de Penly et n° 3 de Cattenom (New detection of cracks on pipes of the safety injection system of reactors n° 1 and n° 2 of the Penly nuclear power plant and n° 3 of Cattenom). IRSN, March 6th, 2023.

[5] "Safety-relevant damage in the safety injection systems of French nuclear power plants", 05/19/2022. https://www.grs.de/en/news/safety-relevant-damage-safety-injection-systems-french-nuclear-power-plants.

[6] J. Bartak and N. Camarcat, "Stress Corrosion Cracking on French NPPs – an overview", 2023. https://www.nucadvisor.com/post/stress-corrosion-cracking-on-french-npps-an-overview.

[7] T. Couvant, C. Varé, J. M. Frund, Y. Thébault, B. Audebert and E. Lemaire, "Susceptibility to IGSCC of cold work austenitic stainless steels in non-polluted primary PWR environment", in Fontevraud 10 - 10th International Symposium on Contribution of Materials Investigations and Operating Experience to LWRs' Safety, Performance and Reliability, 2022, Avignon, France.

[8] Materials Reliability Program: Stress Corrosion Cracking of Stainless Steel Components in Primary Water Circuit Environments of Pressurized Water Reactors (MRP-236, Rev. 1). EPRI, Palo Alto, CA: 3002009967, 2017.

[9] C. Mayor, "EDF Stress Corrosion Cracking Operating Experience Discussion, in Advisory Committeee on Reactor Safeguards (ACRS) Meeting 11/16/2022 on French PWR Safety Injection System Cracking ". November 2022.

[10] "Deciphering the phenomenon of stress corrosion identified on five nuclear reactors (Décryptage du phénomène de corrosion sous contrainte identifié sur cinq réacteurs nucléaires)", Societe Francaise d'Energie Nucleaire - SFEN, January 18th, 2022. https://www.sfen.org/rgn/decryptage-du-phenomene-de-corrosion-sous-contrainte-identifie-sur-cinq-reacteurs-nucleaires/.

[11] "Update on stress corrosion cracking phenomenon: causes, evolutions, reparations", Societe Francaise d'Energie Nucleaire - SFEN, August 1st, 2022. https://sfeninenglish.org/update-on-stress-corrosion-cracking-phenomenon-causes-evolutions-reparations/.

[12] IRSN, "Corrosion sous contrainte : quelles répercussions pour les centrales en France ?", 01/12/2023. https://reperes.irsn.fr/temps-forts/corrosion-sous-contrainte-quelles-repercussions-pour-les-centrales-en-france.

[13] Recommendations Following the Discovery of Intergranular Stress Corrosion Cracks on some French Pressurized Water Reactors. Western European Nuclear Regulators Association (WENRA), November 2023.

[14] IRSN, "Maîtrise de la conformité et du vieillissement des réacterus - Dialogue technique sur le 4ème réexamen périodique des réacterus de 1300 MWe", June 2023. https://www.irsn.fr/sites/default/files/2024-01/13_DT-RP4-1300_IRSN_Conformite-vieillissement_30_06_23_.pdf.

[15] EdF, "Phénomène de CSC détecté sur des portions de tuyauteries de circuits auxiliaires du circuit primaire principal de plusieurs réacteurs nucléaires", 06/07/2022. http://www.hctisn.fr/IMG/pdf/01_edf_csc_-_hctisn_-_220607_vd.pdf.

[16] "Avis IRSN N° 2022-00189", February 14th, 2022. https://www.irsn.fr/sites/default/files/documents/expertise/avis/2022/Avis-IRSN-2022-00189.pdf.
[17] M. Maisonneuve, C. Duhamel, C. Guerre, J. Crepin and I. de Curieres, "Effect of aerated transients on oxidation and SCC of stainless steels in PWR primary water", in 19th International Conference on Environmental Degradation of Materials in Nuclear Power Systems - Water Reactors, EnvDeg 2019, 2019.
[18] P. L. Andresen, "Emerging issues and fundamental processes in environmental cracking in hot water", Corrosion, Vol.64, Iss.5, 2008, pp. 439-464.
[19] K. Fujimoto, T. Iwamura, S. Suzuki, T. Kobayashi and Y. Kikuchi, "SCC Growth rate of cold worked austenitic stainless steel in PWR environment", in AECL/COG/EPRI Workshop: Effects of Cold Work on Stress Corrosion Cracking of Materials in Water Cooled Nuclear Plants, 2007, Toronto, Canada.
[20] Materials Reliability Program: Stress Corrosion Crack Growth Rates in Stainless Steels in PWR Environments (MRP–458). EPRI, Palo Alto, CA: 3002020451, 2022.
[21] B. M. Gordon, D. E. Delwiche and G. M. Gordon, "Service experience of BWR pressure vessels", in American Society of Mechanical Engineers, Pressure Vessels and Piping Division (Publication) PVP 1987.
[22] C. Koehler, "Auxiliary Piping SCC OE Focus Group Update - Industry/NRC Materials Technical Exchange Meeting 6/14/23", June 2023. https://www.nrc.gov/docs/ML2316/ML23160A130.pdf.
[23] Materials Reliability Program: Recommended Factors of Improvement for Evaluating Primary Water Stress Corrosion Cracking (PWSCC) Growth Rates of Thick-Wall Alloy 690 Materials and Alloy 52, 152, and Variants Welds (MRP 386). EPRI, Palo Alto, CA: 3002010756, 2017.
[24] Z. Zhai, M. Toloczko, K. Kruska and S. Bruemmer, "Precursor Evolution and Stress Corrosion Cracking Initiation of Cold-Worked Alloy 690 in Simulated Pressurized Water Reactor Primary Water", Corrosion, Vol.73, Iss.10, 2017, pp. 1224-1236.
[25] Pacific Northwest National Laboratory Investigation of Stress Corrosion Cracking in Nickel-Base Alloys, Volume 3: Stress Corrosion Cracking of Cold-Worked Alloy 690. Pacific Northwest National Laboratory: NUREG/CR-7103 Vol. 3, Nuclear Regulatory Commission, Office of Nuclear Regulatory Research, 2015.
[26] G. S. Was, C. B. Bahn, J. Busby, B. Cui, D. Farkas, M. Gussev, M. Rigen He, J. Hesterberg, Z. Jiao, D. Johnson, W. Kuang, M. McMurtrey, I. Robertson, A. Sinjlawi, M. Song, K. Stephenson, K. Sun, S. Swaminathan, M. Wang and E. West, "How irradiation promotes intergranular stress corrosion crack initiation", Progress in Materials Science, Vol.143, 2024, pp. 101255.
[27] K. J. Stephenson and G. S. Was, "The role of dislocation channeling in IASCC initiation of neutron irradiated stainless steel", Journal of Nuclear Materials, Vol.481, 2016, pp. 214-225.